Summer 2016

Mechanisms of Inverted Seismic Multiplets

Joel Brann
Western Washington University, brannjoel@gmail.com

Mechanisms of Inverted Seismic Multiplets

By

Joel Brann

Accepted in Partial Completion
of the Requirements for the Degree
Master of Science

Kathleen L. Kitto, Dean of the Graduate School

Advisory Committee:

Chair, Dr. Jacqueline Caplan-Auerbach

Dr. Diana Roman

Dr. Bernard Housen

MASTER'S THESIS

In presenting this thesis in partial fulfillment of the requirements for a master's degree at Western Washington University, I grant to Western Washington University the non-exclusive royalty-free right to archive, reproduce, distribute, and display the thesis in any and all forms, including electronic format, via any digital library mechanisms maintained by WWU.

I represent and warrant this is my original work, and does not infringe or violate any rights of others. I warrant that I have obtained written permissions from the owner of any third party copyrighted material included in these files.

I acknowledge that I retain ownership rights to the copyright of this work, including but not limited to the right to use all or part of this work in future works, such as articles or books.

Library users are granted permission for individual, research and non-commercial reproduction of this work for educational purposes only. Any further digital posting of this document requires specific permission from the author.

Any copying or publication of this thesis for commercial purposes, or for financial gain, is not allowed without my written permission.

Joel Brann

June 22, 2016

Mechanisms of Inverted Seismic Multiplets

A Thesis
Presented to
the Faculty of
Western Washington University

In Partial Fulfillment
Of the Requirements for the Degree
Master of Science

by

Joel Brann

June 2016

Abstract

In seismology, multiplets are a series of earthquakes with similar waveforms that are thought to represent a repeating process occurring at the same location. A few studies have previously identified multiplets with waveforms that are inverted relative to one another; here termed inverted multiplets (IMs).For this study, several data sets were searched for additional examples of IMs, including earthquake swarms associated with a volcanic eruption (Mt. Spurr), a dike intrusion (Nechako Basin), dome building (Mt. St. Helens), and times of no volcanic or magmatic activity (Piton de la Fournaise [PDLF], Mt. Spurr). Source mechanisms are determined to describe what could possibly cause this phenomenon. The results suggest there are many ways to produce an IM, but that most of the viable mechanisms relate to dike intrusion. The existence of IMs in a region could be an indicator of a dike intrusion and lead to a greater understanding of subsurface processes.

Table of Contents

Abstract iv
List of Tables vi
List of Figures vi
Introduction 1
Hypothesized Mechanisms of IMs 3
Study Regions 6
Nechako Basin 6
Mt. Spurr 7
Mammoth Mountain 8
Mt. St. Helens 8
Piton de la Fournaise 8
Methods 10
Earthquake Identification 11
Inverted Multiplet Identification 12
Precision of Location Differences 13
Relative Locations 14
Amplitude Calculations 15
Synthetics 17
Nechako Basin 19
Mt. Spurr 21
Mammoth Mountain 22
Mt. St. Helens 24
Piton de la Fournaise 24
Synthetics 25
Discussion 27
Mechanism of Each IM 27
IMs in Other Studies 30
Conclusion 31

List of Tables

Table 1 Nechako 1 IM Differences between P-wave arrival times
Table 2 Nechako 2 IM Differences between P-wave arrival times
Table 3 Mt. Spurr IM Relative Locations
Table 4 Mammoth 1 IM Differences between P-wave arrival times
Table 5 Mammoth 2 IM Differences between P-wave arrival times
Table 6 Synthetic Waveform Correlation Coefficients
Table 7 IM Analysis Results

List of Figures

Figure 1 Multiplets
Figure 2 Three-part model of dike-induced earthquakes and their associated focal mechanisms
Figure 3 Parallel fractures on either side of a dike tip cause opposite senses of motion
Figure 4 Opposite fault motions caused by slip of either side of a solidified plug in a dipping dike
Figure 5 Shear stresses
Figure 6 Two adjacent earthquakes with slightly different strikes
Figure 7 Map of seismic network around the Nechako earthquake swarm
Figure 8 Map of the seismic network surrounding Mt. Spurr
Figure 9 Map of the seismic network surrounding Mammoth Mountain
Figure 10 Waveforms lined up according to the P-wave arrival times
Figure 11 Map view of synthetic seismic array
Figure 12 Seismic recordings of Nechako 1 as recorded by NZ02
Figure 13 Correlograms of Nechako 1 as recorded by NZ02
Figure 14 Occurrence plot of the three clusters of Nechako 1
Figure 15 Seismic recordings of Nechako 2 as recorded by NZ02
Figure 16 Correlograms of Nechako 2 as recorded by NZ02
Figure 17 Occurrence plot of Nechako 2
Figure 18 Seismic recordings of Mt. Spurr IM as recorded by SPU
Figure 19 Correlograms of Spurr IM
Figure 20 Occurrence plot of Spurr IM
Figure 21 Seismic recordings of Mammoth IM 1 as recorded by MGP
Figure 22 Correlograms of Mammoth IM 1
Figure 23 Occurrence plot of Mammoth IM 1
Figure 24 Seismic recordings of Mammoth IM 2 as recorded by MGP
Figure 25 Correlograms of Mammoth IM 2
Figure 26 Occurrence plot of Mammoth IM 2
Figure 27 Thrust and normal synthetic earthquake waveforms
Figure 28 Right lateral and left lateral strike slip synthetic earthquake waveforms
Figure 29 Two synthetic earthquake waveforms with different dips
Figure 30 Two synthetic earthquake waveforms

Introduction

When an earthquake occurs, much of its energy is released in the form of elastic waves. The shape of these waveforms is determined by their focal mechanism (fault orientation and slip direction), the material through which the wave travels, and the response function of the seismometer recording it (Geller and Mueller, 1980). If the same seismometer recorded different earthquakes with identical waveforms, this would indicate the earthquakes each originated at the same location within the subsurface, and were generated by slip along faults with a common orientation and sense of slip.

A group of these similar waveforms is called a multiplet (fig. 1). Multiplets are commonly found in volcanic settings and are often used in conjunction with waveform cross-correlation to better identify arrival times and therefore improve earthquake locations (Got, Frechert, and Klein, 1994). One potential source for multiplet earthquakes is an asperity, or uneven point on a fault, where strain builds up, and some of that strain is repeatedly relieved by slip on the fault (Geller and Mueller, 1980). Whatever the source mechanism, it must be repeatable in order to create the same waveform (Petersen, 2007).

Several previous studies (e.g. Rubin et al., 1998; White et al., 2011; Shelly and Hill, 2011; Cassidy et al., 2011) have identified multiplets in which some waveforms are inverted relative to the others, meaning that they have opposite first motions and continue to move in opposite directions throughout the waveform (fig. 1). For this study, I refer to these multiplets that are composed of two clusters of earthquakes, one inverted to the other, as inverted multiplets (IMs). Rubin et al. (1998) were the first to notice the existence of inverted waveforms within a multiplet recorded during a 1983 diking event beneath Kilauea volcano. This inversion of the waveform could represent a 90° shift in the stress field, causing a failure at the same spot but

with the opposite direction of slip. The authors referred to it as an apparent slip reversal and suggest that it could have been caused by the dike tip entering an area of higher pore pressure, which changed the local stress field (Rubin et al., 1998). This explanation addresses why the stress field in this one particular area would differ from that of the regional stress field.

No other mention of IMs can be found in the literature until the Nechako Basin, British Columbia earthquake swarm of 2007 (Hutchinson and Caplan-Auerbach, 2010; Cassidy et al., 2011). These studies note that earthquakes within that swarm have both compressional P-waves and dilatational P-wave s which, when inverted and cross-correlated, yield high correlation coefficients.

Hypothesized Mechanisms of IMs

One possible explanation for the generation of IMs is a 90^{o} rotation in the direction of the most compressive stress (so that, for example, where a reverse faulting event once occurred, a normal faulting event occurs). This rotation of the stress field has been documented during or prior to many volcanic eruptions (e.g. Jolly, 1994; Waite and Smith, 2004; Roman and Cashman, 2006; Lehto et al., 2010). None of these studies searched for IMs. Roman and Cashman (2006) hypothesize that the rotation of the stress field could be caused by the inflation of a magma-filled dike. Inflation is thought to occur in the direction of regional least compressive stress, which is 90° to the regional most compressive stress. The added stress caused by the inflation could become greater than the regional most compressive stress, making the direction of local most compressive stress 90° to the regional most compressive stress. This mechanism would be characterized by randomly distributed hypocenters away from the walls of the dike (Roman and Cashman, 2006). If a set of earthquakes occurred at the same place before and after the inflation, it could be an IM. Dike inflation could theoretically cause multiple IMs in the same area at the same time. I expect that this phenomenon would not produce both clusters of a single IM to occur contemporaneously. One cluster would occur, and then as the inflation occurs, the inverted cluster would occur. After inflation, the stress field returns to the regional stress field, and could again cause earthquakes similar to the first cluster.

White et al. (2011) present four possible mechanisms that could cause IMs in which the earthquakes do not occur in the exact same location, but could be close enough to exhibit similar waveforms when recorded by the same station. All of these mechanisms are based on slip around dike intrusions rather than stress changes. The first mechanism is that the earthquakes occur on

parallel fractures that form around a propagating dike tip. In this scenario, the sense of motion will be different depending on which side of the dike the fracture is on (fig. 3).

The second possible mechanism proposed by White et al. (2011) is that the IM earthquakes could be occurring on either side of a moving solidified plug within a dipping dike (fig. 4). Such motion of a propagating dike would cause a normal faulting motion on the upper edge of the dike and a reverse faulting motion on the lower edge of the dike. This mechanism can only exist if there is a high-stiffness/incompressible plug with low-stiffness/compressible volumes on either side of it. This is consistent with the findings of Roman and Cashman (2006), who state that stress field rotation seems to be characteristic of magmas that were extensively crystallized during ascent, suggesting that it could be the solidification of the magma that makes it possible for this type of inversion to occur.

The third mechanism proposed by White et al. (2011) is that the dike is broken up into segments that enter different local stress fields which were altered by an earlier intrusion. And finally, White et al. (2011) propose that the earthquakes could occur on fractures on the offsets between the segments which could have opposite motions very close together depending on which side of the fracture the dike fluid motion is on. This would result in the earthquakes occurring on faults oriented about 45° to the dike. These last two mechanisms are illustrated in a figure from Ito and Martel (2002), which shows how multiple dike intrusions can cause a heterogeneous local stress field (fig. 5).

The first, second, and fourth hypotheses of White et al. (2011) cannot be distinguished from each other in seismic data, and are effectively the same process, so I will refer to them collectively as dike motion between two fractures. This mechanism would be characterized by both clusters in the IM occurring contemporaneously at the same location.

Another possibility is that the strike of the fault has shifted slightly to put the seismometer in a different quadrant within the focal sphere (fig. 6). A focal sphere is a projection on a spherical shell surrounding the earthquake. Lines are drawn along the fault plane and orthogonal to the fault plane. This breaks the sphere into four quadrants: two compressional quadrants where the first motion of the waveform is up, and two dilatational quadrants where the first motion is down. The fault could have sufficient complexity that one portion of it strikes in a slightly different direction than a neighboring portion, placing a single seismometer in first one quadrant and then another. Alternatively, there could be two faults that are very close to one another but have slightly different orientations. This shift could cause waveform first motions to be in opposite directions, and if the earthquakes occur very near each other they could still produce similar enough waveforms to be considered multiplets. If this is the case, another seismic station, located farther from the nodal plane, might remain in the same quadrant and would not record the inversion. In this scenario IMs would be characterized by high amplitude S-waves relative to the P-waves in the seismometer that records the inversion because it is near the nodal plane of the focal sphere (Stein and Wysession, 2009).

Study Regions

Data sets of earthquakes occurring in a variety of volcanic and plutonic environments were examined for the occurrence of IMs: an earthquake swarm in 2007 likely caused by an intrusion into the lower crust in the Nechako Basin of British Columbia (Hutchinson and Caplan-Auerbach, 2010; Cassidy et al., 2011), seismic activity during active (1991-1992) and inactive (1999-2000) eruption periods at Mt. Spurr volcano in Alaska, an injection of a pressurized fluid near Mammoth Mountain in California in 2009, a period of Mt. St. Helens' 2004 dome-building eruption, and an active period in 2003 at Piton de la Fournaise (PDLF) volcano, Reunion Island. IMs were previously reported in the Nechako Basin (Cassidy et al., 2011) and Mammoth Mountain (Shelly and Hill, 2011) datasets.

Nechako Basin

An earthquake swarm occurred in 2007 in the Nechako Basin, approximately 20 km west of the Nazko volcanic cone in central British Columbia within the Anahim Volcanic Belt (Cassidy et al., 2011). Volcanic eruptions in this area generally produce basaltic lavas. Due to the high frequency (>5 Hz) nature of the earthquake waveforms and the presence of spasmodic bursts, large amplitude high frequency tremorlike earthquakes, the swarm was inferred to be the result of a magmatic injection into the lowermost crust at about 25-31 km depth (Hutchinson, 2010; Cassidy et al., 2011). Over 1,000 earthquakes were detected within three weeks of the start of the swarm on 16 October and the swarm lasted for approximately two months. Most of the earthquake hypocenters occurred within 5 km of each other with local magnitudes of 1 to 2 (Cassidy et al., 2011). Five 3-component seismometers were installed within an eight mile radius around the epicentral location of the earthquake swarm (fig. 7). Five more seismometers were

located farther away, approximately 20 to 60 miles, but because the earthquakes were so small and deep, the earthquakes were generally detected only by the closest stations. The dbdetect algorithm, part of the Antelope seismic processing system, was used to identify a total of 5,222 earthquakes for this study. The nonideal station distribution and small earthquake size also meant that a fault plane solution could be determined for only one earthquake in the swarm indicating normal faulting about 30-35 km deep (Cassidy et al., 2011).

Mt. Spurr

Mt. Spurr is an active stratovolcano located in south central Alaska, approximately 125 km west of Anchorage. Its most recent eruptive phase compriseda series of three eruptions that occurred in June, August, and September 1992 at the Crater Peak vent (Roman et al., 2004). Seismic activity surrounding these eruptions started in August of 1991 with a swarm of high frequency earthquakes. Two shallow earthquake swarms occurred on June 5, and prior to the eruption on June 27, 1992. Another swarm occurred as the final eruption was ending in September, 1992. Earthquake swarms occurred again in November and late December, 1992. According to Roman et al. (2004), the local stress field was perpendicular to the regional stress field prior to the three eruptions, and during a posteruptive earthquake swarm in November 1992.

I analyzed two different sets of earthquakes located around Mt. Spurr. The first one contains 4,791 earthquakes that occurred during the seismically active period from August 1991 to December 1992. The second dataset contains 571 earthquakes recorded during a two-year quiescent period from 1999 to 2000. Data collected from six vertical component seismometers installed around the volcano were used in this analysis (fig. 8).

Mammoth Mountain

Mammoth Mountain is located on the southwest rim of the Long Valley Caldera in eastern California. It is composed of a cluster of dacitic domes formed ~100-50 ka (Shelly and Hill, 2011). A two-day-long earthquake swarm occurred southwest of the summit on September 29-30, 2009. Using data from four vertical component seismometers that surround Mammoth Mountain to the east of the swarm (fig. 9), I identified 319 earthquakes using a short time average/ long time average (STA/LTA) detection algorithm in MATLAB that determines if an earthquake occurs by comparing the short term average amplitude to the long term average amplitude.

Mt. St. Helens

Mt. St. Helens is an andesitic and dacitic stratovolcano located in southwestern Washington State. In 2004, a phreatic eruption occurred, followed by a prolonged period of dacitic dome building accompanied by a series of highly similar earthquakes, called "drumbeat" earthquakes (Moran et al., 2008). Due to the large number of earthquakes occurring in a brief amount of time, I only examined records of earthquakes occurring between October 16 and 22, 2004. For that interval of time, I identified 1,902 earthquakes using an STA/LTA detection algorithm on station HSR, the closest seismometer to the swarm with the clearest signal, about 1 km southeast of the volcano's center.

Piton de la Fournaise

Piton de la Fournaise (PDLF) is currently one of the most active volcanoes in the world, with 11 eruptions between 2000 and 2003 (Peltier et al., 2005). It is a basaltic shield volcano

located on Reunion Island off the eastern coast of Madagascar. I searched a set of 839 earthquakes that took place within the volcano during a non-eruptive phase from November 1-27, 2003. I used waveform data from the vertical component of the three closest seismometers to the swarm with the clearest signal (stations BOR, FER and SFR) in the search.

Methods

Earthquake waveforms from the six seismic data sets described above were used to identify multiplets and IMs. These earthquake waveforms were then compiled into a separate data set for more in-depth analysis. I cross-correlated all earthquake waveforms in each dataset with one another to identify multiplets and IMs. By calculating the differential P-wave arrival times and S minus P times of the earthquakes in the IMs, I verified that they occurred at the same location. For the dataset that was recorded by 3-component seismometers (Nechako), I rotated the data into their radial and transverse components to identify the maximum amplitude of both the P- and S-waves as well as the ratio of S/P amplitude. P- and S-waves reach their maximum amplitudes in different portions of the focal sphere lying 45° from each other, so the amplitude ratio gives an indication of fault orientation. This amplitude ratio was then compared to every other earthquake within the multiplet. Although focal mechanisms could not be calculated for these earthquakes, this technique allowed me to confirm that each earthquake has a focal mechanism with the same orientation as others in the multiplet.

I reviewed the results of the previously run analyses to determine the most likely cause of each IM. Results were compared with proposed results from hypothesized mechanisms identified in the literature. Additionally, I used the Bouch program within the Seisan seismic analysis package to create synthetic waveforms for different fault orientations (Bouchon, 2003). The correlation coefficients determined by these models were then compared with observed data.

I used the GISMO suite of MATLAB functions (Reyes and West, 2011) to analyze the data in this study. All MATLAB scripts used in this study are included in the Appendix.

Earthquake Identification

I received the Nechako (British Columbia) dataset as continuous seismic data in an Antelope database. I used the Antelope (BRTT, 1996) algorithm dbdetect to identify earthquake arrival times and extract all the earthquakes from this continuous data. This program applies a short time average/ long time average (STA/LTA) algorithm to find events that have specified amplitude thresholds on a number of stations. I used 0.2 seconds for the short time and 5 seconds for the long time and set a detection threshold of 2.5. Where the STA amplitude divided by the LTA amplitude is greater than the detection threshold at multiple stations, an earthquake was detected. For each detected earthquake, I extracted the waveform data from 5 seconds before each detection to 25 seconds after it (this was performed with the MATLAB script "load_nazko_data", available in the appendix). Data were bandpass filtered between 1 and 30 Hz and the waveforms were stored into a correlation object, a GISMO function that can store large numbers of earthquakes to enable quick correlation of many earthquakes.

I obtained data from Mammoth Mountain, California and Mt. St. Helens, WA in the form of continuous raw seismic data in SAC format. I created MATLAB scripts for Mammoth Mountain and Mt. St. Helens, which use a STA/LTA algorithm to identify earthquakes on the stations with the clearest signal (MRD and HSR, respectively). The same parameters used for the Nechako dataset were also utilized for these datasets. The Mammoth Mountain and Mt. St. Helens data were first bandpass filtered from 1 to 30 Hz and the discrete earthquake waveforms were put into a correlation object. I then used the arrival times of those waveforms to collect waveforms from the same earthquakes on each of the other seismometers in each area.

Dr. Diana Roman of the Carnegie Institute of Washington provided me with data sets of discrete earthquakes from Mt. Spurr and PDLF in SAC format. In this format waveforms could be directly placed into correlation objects.

Inverted Multiplet Identification

Cross-correlation was used to analyze the similarity of the earthquake waveforms in this study. This process calculates a correlation coefficient that represents the degree to which one waveform is similar to another waveform. A correlation coefficient of 0 means they are not similar at all and a value of 1 means the two waveforms are identical. In this study, I modified the cross-correlation algorithm to allow for negative correlations. A correlation coefficient of -1 means the two waveforms are identical but inverted. An IM consists of two clusters of earthquakes, one negatively correlated with the other.

Once all of the datasets were stored in correlation objects, I cross-correlated all waveforms in each dataset in order to find multiplets. Normally correlation was performed across the P-waves, except for the Mammoth data, which had very small P-waves so correlation was performed across the S-waves. To find IMs, the xcorr algorithm in the GISMO suite of MATLAB functions (Reyes and West, 2011) had to be edited to allow for the possibility that the best correlation was a negative value. I also adjusted the correlogram command to display correlation coefficients between 1 and -1 instead of between 1 and 0.

I calculated correlation values between -1 and 1 for all events and created a subset of the 20 largest clusters of highly correlated waveforms (positive or negative). A correlogram of the subset was created to show the correlation values within and between the clusters. An IM was identified when one cluster was found to be highly negatively correlated with another cluster.

Once IMs were identified, both clusters were put into a new correlation object to further analyze their spatial and temporal variation.

Precision of Location Differences

Throughout this study and other published studies, earthquakes within multiplets are assumed to have occurred at or very near the same location. The actual distance that is considered very close is not always well constrained. Geller and Mueller (1980) suggest that earthquake waveforms will still appear similar if they are located within ¼ wavelength of each other, where an event's wavelength may be found by dividing the velocity of the wave by its frequency. The earthquakes in this study are VT earthquakes, which generally have a frequency of 5-15 Hz (Lahr et al., 1994). Given an average P-wave velocity of 5800 m/s in the upper crust (Dziewonski & Anderson, 1981), ¼ wavelength is roughly 100 to 300 m, and an average S-wave velocity of 3200 m/s, ¼ wavelength is roughly 50 to 160 m. Therefore, if the earthquakes are any closer together, they will still correlate strongly and the distance between them would be indistinguishable.

Unfortunately, Geller and Mueller (1980) give no reasoning for giving ¼ wavelength as the value and do not define "highly correlated". The synthetics in the current study show that earthquakes with the same focal mechanism located 100 m apart have correlation coefficients of about 0.8, which is similar to the distance given by ¼ wavelength, so for this study I have chosen "very close to one another" to mean within 100 m, and "highly correlated" to mean a correlation coefficient of at least 0.8. This is roughly a difference of 0.02 seconds (or two samples, for data sampled at 100 Hz) of P-wave arrival time.

Relative Locations

I used two methods to determine whether the earthquakes occurred at the same location or at different locations very close to one another. The first method uses the differences in P-wave arrival times at multiple stations and the second method uses the S minus P times at a single station. The similarity of the waveforms suggests that the earthquakes in a multiplet must occur at the same location or very close to one another. These methods were used to determine if the two clusters of an IM are co-located.

The differential P-wave method included noting the difference in P-wave arrival times at three or four different stations for one earthquake. If the difference in P-wave arrival times between all the stations is the same for each waveform, then they must have occurred at the same location (within a region defined by pick uncertainty). I used cross-correlation to line up the waves mathematically at the point where the greatest correlation value exists in the P-wave,allowing for greater precision than what is possible through the traditional method of visually picking the P- and S-wave arrival times. By comparing these differences I am able to determine whether the earthquakes occurred at the same location. This method was used with S-waves instead of P-waves for the Mammoth Mountain IM because P-wave arrival times were difficult to distinguish.

For IMs with discernable P- and S-wave arrival times, the S minus P time method was used. This method involved comparing the P- and S-wave arrival times for each waveform at a single station in each dataset. Since P- and S-waves are generated at the same time and S-waves are slower than P-waves, measuring the difference between the arrival of each wave can tell us the distance between the earthquake and the seismometer. If the S minus P time for each earthquake in a multiplet is the same, then they must have all occurred at the same location

(within the precision allowed by the sample frequency of the digitizer within the seismometer). I first followed the same procedure of lining events up via P-wave cross-correlation. I then lined them up according to where the S-wave correlation value is greatest (fig. 10). The amount of time the waveforms are shifted from where the P-waves correlated highest to where the S-waves correlate the highest is the S-wave offset value. If the S-wave offset value is zero, then the waveform did not need to be shifted relative to the reference waveform, meaning that the S minus P times are the same, and the two associated earthquakes must be co-located.

Amplitude Calculations

Measuring the relative amplitudes of the P- and S-waves can help determine if the same mechanism caused the earthquakes (Hardebeck and Shearer, 2003). S-waves are shear waves, so their energy is strongest along the nodal plane of the fault. P-waves are longitudinal waves, so their energy is strongest at a 45° angle to the fault plane (Stein and Wysession, 2009). So, if a set of earthquakes occur along the same fault plane, their S-wave to P-wave amplitude ratio will be the same. At different azimuths to the fault, or on differently oriented faults, the amplitude ratio will vary.

To accurately measure P and S wave amplitudes, the components of a 3-component seismometer must be rotated to reflect the radial and transverse components of the wave. The radial component of a waveform is oriented in the direction of waveform propagation and therefore is the direction where the P-wave energy is strongest. The transverse component is oriented perpendicular to the direction of propagation, and therefore has the strongest S-wave. Although, if the direction of propagation is mostly vertical, or if the S-wave is vertically

polarized, the vertical component could have the highest and most accurate representation of amplitude.

The Nechako Basin dataset is the only dataset in this study from three-component seismometers, which measure wave motion in north, east, and vertical directions. The other datasets in this study were recorded by one-component vertical seismometers. Radial and transverse components for the Nechako Basin were calculated using the following equations (Stein and Wysession, 2009):

$$R = E\begin{bmatrix} \cos\theta & \sin\theta \\ -\sin\theta & \cos\theta \end{bmatrix}$$

$$T = N\begin{bmatrix} \cos\theta & \sin\theta \\ -\sin\theta & \cos\theta \end{bmatrix}$$

Where R is the radial component, T is the transverse component, N is the north component, E is the east component, and theta is 270 minus the back-azimuth, which is the direction from which the waveform arrives at the seismometer. To determine the back-azimuth, I plotted the radial component multiple times using different back-azimuths ranging from 0 to 180 in 5 degree intervals and plotting all the waveforms. The plot with the strongest P-wave was taken to represent rotation into the orientation of the radial component, and thus this was considered to be the most likely value for the back-azimuth. Using that back-azimuth I was then able to calculate the transverse component. I then measured the amplitudes of the P-waves using the radial component and of the S-waves using the transverse component.

The radial and transverse components yielded P- and S-waves with lower amplitudes than the vertical component, demonstrating that most of the energy is in the vertical component. This is as expected, considering that the location of the earthquakes was found by Cassidy et al.

(2011) to be deep (> 25 km) and directly below the seismometers. I therefore calculated the amplitude ratios of the P- and S-waves using the vertical components. Amplitude ratios were calculated by dividing the highest amplitude of the S-wave by the highest amplitude of the P-wave.

A high S/P ratio shows that the station is located near the strike of the nodal plane. A low S/P ratio shows that the station is approximately 45° to the nodal plane. If the ratio changes on a given station, then the earthquake location or fault orientation changed.

Synthetics

IMs could be caused by a change in strike of the fault, or a change in slip direction on the same fault. To test the effects of fault orientation on seismograms, I calculated synthetic seismograms for a variety of fault orientations and depths.

Synthetic seismograms were created using the Bouchon program in Seisan. Bouchon uses a discrete wavenumber method to calculate the frequency response of the simulated seismometers using a layered model given a source depth, focal mechanism, and station location (Bouchon, 2003). I used a network of 24 virtual seismometers to record the synthetic waveforms created in this study. They were located in three concentric circles with eight seismometers each, located five kilometers, 10 kilometers, and 15 kilometers from the epicenter of the earthquake. Seismometers were placed at 30°, 60°, 120°, 150°, 210°, 240°, 300°, and 330° from the epicenter of the earthquake (fig. 11).

I used five different scenarios which could produce inverted waveforms in order to compare them to the real data. The first scenario was a 45°-dipping fault first moving in pure thrust motion, then in a pure normal motion. The second scenario was a vertical strike slip fault

moving in pure right lateral, then pure left lateral motions. Third was a vertical right lateral strike slip fault with a change of strike from 20° to 40°. The fourth scenario was a thrust fault with a change of dip from 15° to 45° to 80°. Also, thrust and normal faults at depths of 14 km, 14.1 km, and 15 km were created to determine the change in correlation with a difference in location.

If the inversion was created by a slight change in orientation of the fault, then inversion would be expected to take place in seismometers that switched quadrants within the focal sphere, but not in others that stayed in the same quadrant. The array of seismometers surrounding the earthquake was used to determine the difference in response of the instruments depending on where they are located relative to the fault orientation. A 180° change in slip direction is expected to show an inversion in all seismometers in the array. Earthquakes at the different depths were used to determine the amount of change in a waveform given a change in source location.

Results

Five IMs were identified in this study. Two IMs were found in the Nechako Basin dataset, two were found in the Mammoth Mountain dataset, and one was found during the active period of Mt. Spurr. No IMs were found at Mt. St. Helens, PDLF, or during the quiet period of Mt. Spurr.

Nechako Basin

Nechako 1

The first IM identified in the Nechako Basin earthquake swarm, hereafter called Nechako 1, contained 77 earthquakes. Sixty of the earthquakes had one first motion and 17 had the opposite first motion (fig. 12). The 60 earthquakes can be further divided into two clusters so that Nechako 1 appears to have three distinct clusters of earthquakes. The first two clusters are positively correlated in the P-waves with the same first motions, but the S-waves in the second cluster have very low amplitudes compared to the first and third cluster (fig. 12). The third cluster has P-waves that are negatively correlated with the first two. Finally, the S-waves in the third cluster are positively correlated with the S-waves in the first cluster, while the P-waves are negatively correlated (fig. 13).

The earthquakes are large enough to be distinguishable above the background noise on four of the 10 local seismometers: NZ02, NZ03, NZ04, UBRB, SULB, and some are distinguishable on NZ01. All of the seismometers recorded the first motion in the first and second set of earthquakes as up and the third set of earthquakes showed a down first motion, except SULB, which shows the opposite in all events. Of the events in Nechako 1, cluster 1

occurred between October 30 and 31, 2007. Cluster 2 occurred October 29 to November 1, 2007. Cluster 3 occurred between noon on October 29 and the morning of October 30, 2007 (fig. 14).

S/P amplitude ratios were calculated for the earthquakes in each set. The mean amplitude ratios for the three sets, with standard deviations in parentheses, are 0.99 (0.29), 0.52 (0.52), and 1.05 (0.14), respectively. A t-test shows that the amplitude ratio for the second set is significantly lower than the other two sets at a 95% confidence level, suggesting that they might have been caused by a different fault orientation.

Waveforms recorded by NZ02, NZ03, NZ04, and UBRB were clear enough to determine precise arrival times, so they were used in the differential P-wave arrival time method to determine relative location. The S minus P time method was also performed using NZ02. There is no difference in arrival times (> 0.01 seconds) in either method (Table 1). Therefore, both clusters must have all occurred at the same location, or within 100m.

Nechako 2

The second IM in the Nechako dataset (Nechako 2) contained 49 earthquakes. Cluster 1 includes twenty-three earthquakes with one first motion and cluster 2 includes 26 with the opposite first motion (fig. 15). All the earthquakes are distinguishable above background noise on NZ02, UBRB, SULB, and some are distinguishable on NZ01, NZ04, TALB, and THMB. All show first motions of down in the first set and up in the second set, except THMB, which shows the opposite. P-wave correlations at NZ02 are fairly strong within the clusters but not very strong between the clusters (fig. 16). This is probably because the P-waves are very weak at all stations and in some cases indistinguishable from the background noise. Correlations are very strong in the S-waves within the clusters and are strongly negatively correlated between the clusters. The

first cluster occurred from October 21 to 24, 2007. The second cluster occurred from October 21 to 26, 2007; both clusters occurred contemporaneously (fig. 17).

Amplitude ratios were also calculated for this IM. The mean amplitude ratios of the two clusters are 1.00 and 1.13 with standard deviations of 0.80 and 0.79 respectively. A t-test indicates that these two means are not significantly different at 95% confidence and therefore the two clusters could be caused by the same focal mechanism with opposite motions.

Waveforms recorded by NZ02, UBRB, and SULB were clear enough to determine precise S-wave arrival times, so they were used in the differential S-wave arrival time method to determine relative location. The S minus P method was not used in this IM due to uncertain P-wave arrival times in many of the waveforms. There is no difference in arrival times in the differential S-wave arrival time method. Therefore, the earthquakes must have all occurred at approximately the same location.

Mt. Spurr

The IM identified in the Mt. Spurr dataset consists of 18 earthquakes (fig. 18). Five earthquakes had one first motion and 13 had the opposite first motion. P-wave and S-wave correlations are very high (coefficients > +/- 0.8) in both clusters (fig. 19). The earthquakes are distinguishable on six seismometers in the region. The clearest waveforms appear in stations CRP and SPU, which show a down first motion in the first cluster. CGL, CKN, and CKL are less clear and show an up first motion in the first cluster. Station BGL is not quite as clear, but seems to show no inversion; earthquakes in both sets have an up first motion. The first set includes one earthquake which occurred in April 1992 and four which occurred between October 8 and 18,

1992. The second set occurred from May 6 to 10, 1992 with one earthquake in November, 1992 (fig. 20).

Waveforms recorded by SPU, CRP, and CKL were clear enough to determine precise P-wave arrival times, so they were used in the differential P-wave arrival time method to determine relative location. There is some difference in the arrival times (Table 3). The first method shows differences of only 0.01 and 0.02 seconds, a difference of only one or two sample points. The earthquake that occurred in November has a differential P-wave arrival time of 0.05 to 0.08 seconds later than the others, depending on the station. Upon closer examination, it can be seen that this waveform has a very different S-wave than the others and a lower correlation coefficient (0.58), so it can be removed from the IM.

The S minus P time method was also performed using SPU. This second method shows the same results with the second cluster, but the first cluster shows differences of 0.03 to 0.05 seconds. The November earthquake had an S-P time difference of 0.18 seconds, confirming that it does not belong in the IM. Both methods show that the relative locations of earthquakes do not progressively change in one direction, but they oscillate around the point where the majority of earthquakes occur. The earthquakes in this IM are very close, but perhaps did not occur at the same location. Based on the difference in arrival times of 0.01-0.05s, they appear to have occurred within 50-250 m of each other.

Mammoth Mountain

Mammoth 1

The first IM identified in the Mammoth Mountain earthquake swarm, Mammoth 1, contained 24 earthquakes with one first motion and 12 with the opposite first motion (fig 21).

The earthquakes are distinguishable on four seismometers: MGP, MRD, MDPB, and MMP. All show the first motion in the first cluster as up and the second cluster as down. P-wave correlation among the earthquakes in the IM are very high (>0.8), but S-wave correlations are low because S waves are only faintly visible, although a few S-waves in the second cluster seem to be positively correlated to those in the first cluster (fig. 22). Both sets occurred between the evening of September 29, 2009 and the morning of September 30, 2009 (fig. 23).

Waveforms recorded by MGP and MRD were clear enough to determine precise P-wave arrival times, so they were the only stations used in the differential P-wave arrival time method to determine relative location. The S minus P time method was not performed due to indiscernible S-wave arrivals. There is a 0.03 second difference in arrival times between the two stations (Table 4). Therefore, I infer that the earthquakes occurred in slightly different locations. This difference could result in a change in distance of about 150-200 meters, assuming a P-wave velocity of 5800 m/s a tomographic image of Mammoth Mountain at -1.75 km to 0.25 km above sea level (Dawson et al., 2016).

Mammoth 2

The second IM, Mammoth 2, contained 7 earthquakes with an up first motion on all four seismometers and 12 earthquakes with a down first motion (fig. 24). The P-waves correlate very strongly (>0.8) in each cluster and strongly negatively to each other (fig. 25). The S-waves correlate somewhat less strongly in the first cluster (>0.6) and not at all in the second cluster, since the second cluster does not have discernable S-waves. The first set occurred between 3:00 and 7:00 pm on September 29, 2009. The second set occurred between 6:00 pm on September 29 and 12:40 am on September 30, 2009 (fig. 26).

Waveforms recorded by MGP and MRD were clear enough to determine precise P-wave arrival times, so they were the only stations used in the differential P-wave arrival time method to determine relative location. The S minus P time method was not performed due to indiscernible S-wave arrival times. There is a difference in arrival times between the two stations (Table 4). They show a difference of 0.01 to 0.05 seconds in most waves. Two waveforms have a difference of greater than 0.25 seconds. Therefore, the earthquakes occurred in different locations.

The Mammoth Mountain earthquakes have previously been located using traditional locating methods. Locations were obtained from the Northern California Seismic Network (NCSN) catalog (NCEDC, 2014). The catalog locations also include differences in location of up to one km between these earthquakes. These locations do not cluster as tightly as they should, given that they are multiplets, but that is likely due to uncertainties associated with the catalog's locating methods.

Mt. St. Helens

No IMs were found in the Mt. St. Helens dataset. Because my search only included one seismometer at this location, I cannot rule out the change in strike mechanism as a possibility. That mechanism could include a seismometer that does not record an inversion. Many multiplets were present in the data, but none inverted.

Piton de la Fournaise

No IMs were found in the Piton de la Fournaise dataset. This could be because my search was limited to the data available to me during a non-eruptive phase, which was a period between

eruptions in November 2003. I cannot rule out the possibility that IMs are associated with eruptions, or that they may have occurred at other times.

Synthetics

Synthetic waveforms were created to explore a variety of scenarios that could produce inversion of waveforms as documented in these seismic data sets. Waveforms were created with differing slip motion, strike, and dip, and also at different depths to determine the amount of difference in the waveforms with the earthquakes being different distances apart. The changes were made with all other parameters being equal to allow for direct comparisons. Synthetic waveforms were recorded by an array of seismic stations situated around the epicenter (fig. 11).

Changing rake by 180 degrees was found to create IMs on all stations. The reverse faulting event and normal faulting event have a correlation coefficient of -1 on all seismometers, as expected (fig. 27; Table 6). The same is true for right lateral and left lateral strike slip earthquakes (fig. 28; Table 6).

A change in strike alone did not change the waveforms on any station in the network, possibly due to a limitation of the program. The program does not vary the amplitude of the P- and S-waves according to position of the seismometer relative to the earthquake, which is the biggest change expected with a change in strike. The hypothesis that a slight change in strike could appear as reverse motion on the fault depending on the distribution of the seismometers is therefore not demonstrated here with the synthetics. It is however well understood that seismometers near the nodal plane of an earthquake record stronger S-waves than seismometers away from a nodal plane, and if that nodal plane moves from one side of the seismometer to the other the first motion will change (Stein and Wysession, 2009).

A change in dip of the fault can also be used to represent a change in fault orientation. Changes in the dip greatly decreased the correlation coefficients. Dips of 15°, 45°, and 80° were used. Even with a 30° change in dip, the correlation coefficients were not high enough to meet the 0.8 threshold used in this study (fig. 29; Table 6) and smaller changes did not clearly show different first motions. Each station showed the same correlation coefficients, but negative for those stations that switched quadrants. Changes in dip would only be expected to cause an inversion if it places a seismometer on either side of a nodal plane, but it would have to be a subtle change in order for the correlation to be high enough to be considered a multiplet.

I also created synthetic waveforms from earthquakes different distances apart to determine how far apart earthquakes can be from each other and still have similar enough waveforms to be considered multiplets. Correlation coefficients decrease the farther the earthquakes are from each other. This is shown by the synthetic waveforms created at different depths (fig. 30; Table 6). The waveform at 14 km depth and the waveform at 14.1 km depth, with all other parameters equal, have a correlation coefficient of 0.8 on all stations in the network. Therefore, the maximum distance earthquakes can be apart and still meet the 0.8 threshold for this study is 100 m if correlating over the entire waveform given the model velocity structure. Interpolating between the scenario at 100 m apart and the scenario at 900 m apart, the correlation coefficient for correlating over just the P-waves will reach 0.8 at about 500 m apart. As distance between the earthquakes increase, the S-wave correlation appears to decrease faster than P-wave correlation. With motion in the opposing directions, the coefficients are the same, but negative.

Discussion

Four possible mechanisms which could cause IMs would each have different attributes (Table 7). If an IM was caused by an inflating dike (Roman and Cashman, 2006) or a subsequent dike intrusion (White et al., 2011), the two clusters that make up the IM would occur at different times and at the same location. If the IM was caused by dike motion between two fractures (White et al., 2011), the two clusters would occur contemporaneously but at slightly different locations that may be indiscernible from each other. If the IM was caused by a slight change in the fault plane, the two clusters would occur at slightly different locations, they would have different amplitude ratios, and the inversion might not appear at all seismic stations. However, if there are few stations or if their distribution is poor, the inversion may be captured on all of the stations.

Mechanism of Each IM

Nechako

Nechako 1 includes three clusters of earthquakes. Based on S-P times and P arrival times, all three clusters appear to have occurred at the same location. The first and third clusters have the same amplitude ratios, indicating that they have the same fault orientation. Clusters 1 and 3 have inverted P-waves and non-inverted S-waves (correlation coefficient approximately 0.7). Because no other instances of this have been found, I have no explanation to describe how the S-waves would not invert with the P-waves, and this observation is left for future investigation.

Cluster 2 has a different mean amplitude ratio than the other two, indicating different fault orientation. The different ratio indicates that the stress field is not shifting causing a slip reversal; it is the strike of the fault that is shifting. This could be two nearby faults or a slightly

different place on the same fault with complexities in it that change the strike. Due to the close spatial distribution of the stations, all of the stations recorded an inversion. It is plausible that none of the stations were located in the portion of the focal sphere where an inversion was not recorded.

Clusters 1 and 3 did not occur contemporaneously; cluster 3 occurred first, followed by cluster 1. This suggests that after cluster 3 occurred, the stress field changed. The change must have been very localized, because it did not affect cluster 2, which overlaps both the other clusters in time.

Nechako 2 has very small P-waves at all available stations, so it does not correlate very well in the P-wave, but the strong S-waves correlate very well. There is no distinguishable difference in the location of the earthquakes in this IM, so they either occurred at the same location or very close to one another. Cluster 1 mostly all occurred within one day and cluster 2 was spread out over four days, both before and after cluster 1, including the day cluster 1 occurred.

No seismicity has been known to occur previously in this area (Cassidy et al., 2011), so the IMs are unlikely to be caused by a previous intrusion that changed the local stress field before this earthquake swarm. The inflating dike hypothesis is also ruled out because both clusters occurred contemporaneously. The most likely cause of these two IMs is that the earthquakes are occurring from dike motion between two fractures since they occur contemporaneously and the earthquake swarm is thought to have been caused by an intrusion (Cassidy et al., 2011). Cluster 2 in Nechako 1 can be explained by one of the fractures having a slightly different strike than the others.

Mt. Spurr

The Mt. Spurr IM correlates very well in the P- and S-waves, although there are some differences in the event locations. The earthquakes in cluster two occurred very close to one another, but there are some small differences between locations in cluster one. One seismometer out of the six does not show an inversion. The two clusters do not occur at the same time; cluster 1 occurs months apart from most of cluster 2.

Roman et al. (2004) found that the local stress field around Crater Peak, where the earthquakes occurred, was perpendicular to the regional stress field prior to three eruptions, which occurred in June, August, and September of 1992. Immediately after the eruptions, the local stress field was parallel to the regional stress field. This suggests that the eruptions were the cause of the change in stresses. One cluster of the IM occurred before the eruptions and one occurred after the eruptions, consistent with this change. Bearing the findings of Roman et al. (2004) in mind, and the fact that all but one seismometer showed the shift, I argue that the movement of magma caused the dike to inflate, causing a very nearly 90° shift in the local stress field.

Mammoth Mountain

Mammoth 1 correlates very well in the P-wave but not in the S-wave because the waveforms lack significant S-waves that can be correlated. All the earthquakes occurred at the same location. The two clusters occurred contemporaneously, so it cannot be the inflation or subsequent intrusion hypotheses.

Mammoth 2 also only correlates well in the P-waves due to a lack of S-waves. The two clusters occur at the same location, mostly at different times, except for one earthquake that

occurs while the other cluster is happening. This one earthquake is inconsistent with the inflating dike and subsequent intrusion hypotheses.

Shelly and Hill (2011) concluded that the earthquake swarm was caused by movement of a supercritical fluid (CO_2). It is possible that these two IMs are caused by fluid motion between two fractures.

IMs in Other Studies

I have applied the hypothesized mechanisms in this study to previous studies that found IMs. Rubin and Gillard (1998) do not provide the dates and times of the earthquakes in the IM they discovered under Kilauea, but they do state that there is a single station that does not record an inverted multiplet, where at least four stations did record it. Therefore, that IM is likely caused by a slight shift in the strike of the fault, which keeps one station still in the same quadrant, rather than the 180° change in slip that they posited.

White et al. (2011) state that the focal mechanisms of earthquakes occurring at the same location in an earthquake swarm under Iceland flip rapidly, within minutes of each other. It seems likely that the IM was caused by dike motion between two fractures because of the frequent orientation change. White et al. did not analyze the earthquake waveforms, only their moment tensor solutions, so they did not identify changes in wave amplitude, or whether the inversion was recorded on all stations. Thus it is possible that it was caused by a slight shift in the strike of the fault, but models related to diking appear to be more likely.

Roman et al. (2004) discuss a pair of earthquakes at Mt. Spurr which occurred within two hours of each other in 1992, which had approximately the same location and opposite fault-plane solutions, but very different waveforms. This is an interesting case, because the synthetics suggest that these two waveforms should be identical but inverted. Earthquakes can appear

different if they are located as little as 100 m apart, so a small amount of location error or a highly heterogeneous environment could make different source locations appear co-located.

Conclusion

Most of the IMs in this study were found to have occurred as a result of a dike intrusion. The only exception to this is Mammoth Mountain which, according to Shelly and Hill (2011), was caused by ascending CO_2. The three datasets where no IMs were found (Mt. St. Helens, PDLF, and the quiet period of Mt. Spurr) occurred at times and locations where no intrusions were occurring. The Mt. St. Helens seismicity was associated with dome extrusion. The earthquakes are thought to have been caused by stick-slip activity on the sides of an extruding spine (Iverson et al., 2006) and not from any dike intrusions. This action could theoretically create IMs from motion between two fractures, but the spine would have to be less than approximately 100 m across for the earthquakes to be close enough to be multiplets. PDLF and Mt. Spurr are both active volcanoes, but IMs were found only during an eruptive period at Mt. Spurr and not during the quiescent period. An eruptive period of PDLF was not used in this study.

The existence of IMs in a given dataset could therefore be used as an indicator that an earthquake swarm is caused by a dike intrusion. This knowledge could be used as evidence of future seismic or volcanic activity.

References

Bouchon, M., 2003. A Review of the Discrete Wavenumber Method: Pure and Applied Geophysics, v. 160, p. 445-465.

Boulder Real Time Technologies (BRTT), 1996. Antelope Environmental Monitoring Software, http://www.brtt.com/software.html.

Cassidy, J.F., Balfour, N., Hickson, C., Kao, H., White, R., Caplan-Auerbach, J., Mazzotti, S., Rogers, G.C., Al-Khoubbi, I., Bird, A.L., Esteban, L., Kelman, M., Hutchinson, J., and McCormack, D., 2011. The 2007 Nazko, British Columbia, Earthquake Sequence: Injection of Magma Deep in the Crust beneath the Anahim Volcanic Belt. Bulletin of the Seismological Society of America, 101: 1732-1741.

Dawson, P., B. Chouet, and A. Pitt (2016), Tomographic image of a seismically active volcano: Mammoth Mountain, California, J. Geophys. Res. Solid Earth, 121, 114–133, doi:10.1002/2015JB012537.

Dziewonski, A.M., and Anderson, D.L., 1981, Preliminary reference Earth model: Physics of the Earth and Planetary Interiors, v. 25, no. 4, p. 297–356, doi: 10.1016/0031-9201(81)90046-7.

Frémont, M.-J., and Malone, S.D., 1987, High Precision Relative Locations of Earthquakes at Mount St. Helens, Washington: Journal of Geophysical Research, v. 92, no. B10, p. PP. 10,223-10,236.

Geller, R.J., and Mueller, C.S., 1980, Four similar earthquakes in central California: Geophysical Research Letters, v. 7, no. 10, p. PP. 821–824, doi: 198010.1029/GL007i010p00821.

Got, J.L., Frechert, J., and Klein, F.W., 1994, Deep fault plane geometry inferred from multiplet relative relocation beneath the south flank of Kilauea: Journal of Geophysical Research, v. 99, no. B8, p. 15.

Hardebeck, J.L. and Shearer, P.M., 2003. Using S/P Amplitude Ratios to Constrain the Focal Mechanisms of Small Earthquakes: Bulletin of the Seismological Society of America, v. 93, no. 6, p. 2434-2444.

Hutchinson, J.A., and Caplan-Auerbach, J., 2010, New perspectives on the 2007 seismic swarm in the Anahim Volcanic Belt, British Columbia, from earthquake cross-correlation and high-resolution relocations: AGU Fall Meeting Abstracts, v. -1, p. 2039.

Iverson, R. M., Dzurisin, D., Gardner, C. A., Gerlach, T. M., LaHusen, R. G., Lisowski, M., ... & Pallister, J. S. (2006). Dynamics of seismogenic volcanic extrusion at Mount St Helens in 2004–05. *Nature*, *444*(7118), 439-443.Jolly, A. D., Page, R. A., & Power, J. A. (1994). Seismicity and stress in the vicinity of Mount Spurr volcano, south central

Alaska. *Journal of Geophysical Research: Solid Earth (1978–2012)*, *99*(B8), 15305-15318)

Lahr, B.A., Chouet, C.D., Stephens, J.A., Power, R.A., Earthquake classification, location, and error analysis in a volcanic environment: implications for the magmatic system of the 1989-1990 eruptions at Redoubt Volcano, Alaska. *Journal of Volcanology and Geothermal Research* 62 (1994) 137-151

Lehto, H. L., Roman, D. C., & Moran, S. C. (2010). Temporal changes in stress preceding the 2004–2008 eruption of Mount St. Helens, Washington. *Journal of Volcanology and Geothermal Research*, *198*(1), 129-142)

Moran, S.C., Malone, S.D., Qamar, A.I., Thelen, W.A., Wright, A.K., and Caplan-Auerbach, J., 2008, Seismicity Associated with Renewed Dome Building at Mount St. Helens, 2004-2005: US Geological Survey professional paper, , no. 1750, p. 27–60.

NCEDC, 2014, Northern California Earthquake Data Center. UC Berkeley Seismological Laboratory. Dataset. doi:10.7932/NCEDC.

Peltier, A., Ferrazzini, V., Staudacher, T., Bachelery, P., 2005. Imaging the dynamics of dyke propagation prior to the 2000–2003 flank eruptions at Piton de La Fournaise, Reunion Island, Geophys. Res. Lett., 32, L22302, doi: 10.1029/2005GL023720.

Petersen, Tanja, Swarms of repeating long-period earthquakes at Shishaldin Volcano, Alaska, 2001–2004: Journal of Volcanology and Geothermal Research, 166 (2007), p. 177-192.

Reyes, C.G., and West, M.E., 2011, The Waveform Suite: A Robust Platform for Manipulating Waveforms in MATLAB: Seismological Research Letters, v. 82, no. 1, p. 104 -110.

Roman, D.C., Moran, S.C., Power, J.A., Cashman, K.V., 2004. Temporal and Spatial Variation of Local Stress Fields before and after the 1992 Eruptions of Crater Peak Vent, Mount Spurr Volcano, Alaska. Bulletin of the Seismological Society of America, 94: 2366-2379.

Roman, D.C., and Cashman, K.V., 2006, The origin of volcano-tectonic earthquake swarms: Geology, v. 34, no. 6, p. 457–460, doi: 10.1130/G22269.1.

Rubin, A., Gillard, D., Got, J.L., 1998. A reinterpretation of seismicity associated with the January 1983 dike intrusion at Kilauea Volcano, Hawaii. Journal of Geophysical Research, 103: 10, 003-10,015.

Sapin, M., Hirn, A., Lepine, J. C., and Nercessian, A., 1996, Stress, failure, and fluid flow deduced from earthquakes accompanying eruptions at Piton de la Fournaise Volcano: Journal of Volcanology and Geothermal Research, v. 70, p. 145–167, doi: 10.1016/0377-0273(95)00043-7.

Shelly, D.R., and Hill, D.P., 2011, Migrating swarms of brittle-failure earthquakes in the lower crust beneath Mammoth Mountain, California: Geophysical Research Letters, v. 38, no. 20, p. L20307, doi: 10.1029/2011GL049336.

Stein, S., and Wysession, M. 2009. An introduction to seismology, earthquakes, and earth structure. John Wiley & Sons.

Waite, G. P., & Smith, R. B. (2004). Seismotectonics and stress field of the Yellowstone volcanic plateau from earthquake first-motions and other indicators. *Journal of Geophysical Research: Solid Earth (1978–2012)*, *109*(B2).

Waldhauser, F., Ellsworth, W., and Cole, A., 1999. Slip-parallel seismic lineations on the Northern Hayward Fault, California. Geophysical Research Letters, v. 26, no. 23, p. 3525-3528.

White, R.S., Drew, J., Martens, H.R., Key, J., Soosalu, H., Jakobsdóttir, S.S., 2011. Dynamics of dyke intrusion in the mid-crust of Iceland. Earth and Planetary Science Letters, 304: 300-312.

TABLES

Table 1: Nechako 1 IM Differences between P-wave arrival times

Set	NZ02 Arrival Times	NZ04 Arrival Times	Difference	Offset (sec)
1	30-Oct-2007 11:20:02	30-Oct-2007 11:20:02	0.000	0.000
1	30-Oct-2007 14:11:04	30-Oct-2007 14:11:04	0.000	0.000
1	30-Oct-2007 14:14:20	30-Oct-2007 14:14:20	0.000	0.000
1	30-Oct-2007 14:24:03	30-Oct-2007 14:24:03	0.000	0.000
1	30-Oct-2007 15:12:16	30-Oct-2007 15:12:16	0.000	0.000
1	30-Oct-2007 16:52:16	30-Oct-2007 16:52:16	0.000	0.000
1	31-Oct-2007 01:32:59	31-Oct-2007 01:32:59	0.000	0.000
1	31-Oct-2007 05:03:29	31-Oct-2007 05:03:29	0.000	0.000
2	29-Oct-2007 14:43:01	29-Oct-2007 14:43:01	0.000	0.000
2	29-Oct-2007 14:55:59	29-Oct-2007 14:55:59	0.000	0.000
2	30-Oct-2007 04:02:42	30-Oct-2007 04:02:42	0.000	0.000
2	30-Oct-2007 05:30:09	30-Oct-2007 05:30:09	0.000	0.000
2	30-Oct-2007 06:22:13	30-Oct-2007 06:22:13	0.000	0.000
2	30-Oct-2007 06:26:25	30-Oct-2007 06:26:25	0.000	0.000
2	30-Oct-2007 06:28:15	30-Oct-2007 06:28:15	0.000	0.000
2	30-Oct-2007 06:30:17	30-Oct-2007 06:30:17	0.000	0.000
2	30-Oct-2007 06:30:13	30-Oct-2007 06:30:13	0.000	0.000
2	30-Oct-2007 07:10:48	30-Oct-2007 07:10:48	0.000	0.000
2	30-Oct-2007 07:28:21	30-Oct-2007 07:28:21	0.000	0.000
2	30-Oct-2007 07:48:36	30-Oct-2007 07:48:36	0.000	0.000
2	30-Oct-2007 10:08:17	30-Oct-2007 10:08:17	0.000	0.000
2	30-Oct-2007 10:30:52	30-Oct-2007 10:30:52	0.000	0.000
2	30-Oct-2007 10:31:37	30-Oct-2007 10:31:37	0.000	0.000

Set	NZ02 Arrival Times	NZ04 Arrival Times	Difference	Offset (sec)
2	30-Oct-2007 10:39:03	30-Oct-2007 10:39:03	0.000	0.000
2	30-Oct-2007 10:44:38	30-Oct-2007 10:44:38	0.000	0.000
2	30-Oct-2007 10:48:05	30-Oct-2007 10:48:05	0.000	0.000
2	30-Oct-2007 11:00:18	30-Oct-2007 11:00:18	0.000	0.000
2	30-Oct-2007 11:02:39	30-Oct-2007 11:02:39	0.000	0.000
2	30-Oct-2007 11:03:38	30-Oct-2007 11:03:38	0.000	0.000
2	30-Oct-2007 11:24:51	30-Oct-2007 11:24:51	0.000	0.000
2	30-Oct-2007 11:30:00	30-Oct-2007 11:30:00	0.000	0.000
2	30-Oct-2007 11:33:14	30-Oct-2007 11:33:14	0.000	0.000
2	30-Oct-2007 11:37:47	30-Oct-2007 11:37:47	0.000	0.000
2	30-Oct-2007 11:38:44	30-Oct-2007 11:38:44	0.000	0.000
2	30-Oct-2007 12:09:58	30-Oct-2007 12:09:58	0.000	0.000
2	30-Oct-2007 12:17:10	30-Oct-2007 12:17:10	0.000	0.000
2	30-Oct-2007 12:24:33	30-Oct-2007 12:24:33	0.000	0.000
2	30-Oct-2007 12:36:00	30-Oct-2007 12:36:00	0.000	0.000
2	30-Oct-2007 12:45:42	30-Oct-2007 12:45:42	0.000	0.000
2	30-Oct-2007 13:06:48	30-Oct-2007 13:06:48	0.000	0.000
2	30-Oct-2007 13:43:30	30-Oct-2007 13:43:30	0.000	0.000
2	30-Oct-2007 14:06:44	30-Oct-2007 14:06:44	0.000	0.000
2	30-Oct-2007 14:18:14	30-Oct-2007 14:18:14	0.000	0.000
2	30-Oct-2007 14:21:15	30-Oct-2007 14:21:15	0.000	0.000
2	30-Oct-2007 14:26:49	30-Oct-2007 14:26:49	0.000	0.000
2	30-Oct-2007 14:49:18	30-Oct-2007 14:49:18	0.000	0.000
2	30-Oct-2007 15:13:43	30-Oct-2007 15:13:43	0.000	0.000

Set	NZ02 Arrival Times	NZ04 Arrival Times	Difference	Offset (sec)
2	30-Oct-2007 15:19:13	30-Oct-2007 15:19:13	0.000	0.000
2	30-Oct-2007 15:32:24	30-Oct-2007 15:32:24	0.000	0.000
2	30-Oct-2007 17:28:01	30-Oct-2007 17:28:01	0.000	0.000
2	31-Oct-2007 00:33:52	31-Oct-2007 00:33:52	0.000	0.000
2	31-Oct-2007 01:54:51	31-Oct-2007 01:54:51	0.000	0.000
2	31-Oct-2007 02:31:45	31-Oct-2007 02:31:45	0.000	0.000
2	31-Oct-2007 02:32:17	31-Oct-2007 02:32:17	0.000	0.000
2	31-Oct-2007 03:14:42	31-Oct-2007 03:14:42	0.000	0.000
2	31-Oct-2007 04:14:30	31-Oct-2007 04:14:30	0.000	0.000
2	31-Oct-2007 07:08:16	31-Oct-2007 07:08:16	0.000	0.000
2	31-Oct-2007 13:43:25	31-Oct-2007 13:43:25	0.000	0.000
2	31-Oct-2007 14:13:05	31-Oct-2007 14:13:05	0.000	0.000
3	01-Nov-2007 02:13:11	01-Nov-2007 02:13:11	0.000	0.000
3	29-Oct-2007 12:21:29	29-Oct-2007 12:21:29	0.000	0.000
3	29-Oct-2007 12:45:01	29-Oct-2007 12:45:01	0.000	0.000
3	29-Oct-2007 13:06:03	29-Oct-2007 13:06:03	0.000	0.000
3	29-Oct-2007 13:10:42	29-Oct-2007 13:10:42	0.000	0.000
3	29-Oct-2007 13:31:36	29-Oct-2007 13:31:36	0.000	0.000
3	29-Oct-2007 13:32:27	29-Oct-2007 13:32:27	0.000	0.000
3	29-Oct-2007 14:05:29	29-Oct-2007 14:05:29	0.000	0.000
3	29-Oct-2007 14:16:57	29-Oct-2007 14:16:57	0.000	0.000
3	29-Oct-2007 14:26:41	29-Oct-2007 14:26:41	0.000	0.000
3	29-Oct-2007 14:35:49	29-Oct-2007 14:35:49	0.000	0.000
3	29-Oct-2007 14:53:46	29-Oct-2007 14:53:46	0.000	0.000

Set	NZ02 Arrival Times	NZ04 Arrival Times	Difference	Offset (sec)
3	29-Oct-2007 16:30:34	29-Oct-2007 16:30:34	0.000	0.000
3	29-Oct-2007 17:45:20	29-Oct-2007 17:45:20	0.000	0.000
3	29-Oct-2007 18:49:37	29-Oct-2007 18:49:37	0.000	0.000
3	29-Oct-2007 20:49:28	29-Oct-2007 20:49:28	0.000	0.000
3	30-Oct-2007 04:29:12	30-Oct-2007 04:29:12	0.000	0.000
3	30-Oct-2007 06:08:22	30-Oct-2007 06:08:22	0.000	0.000

Table 2: Nechako 2 IM Differences between P-wave arrival times

Set	NZ02 Arrival Times	THMB Arrival Times	Difference	Offset (sec)
1	21-Oct-2007 08:09:33	21-Oct-2007 08:09:33	00:00:00.010	0.000
1	22-Oct-2007 03:30:47	22-Oct-2007 03:30:47	00:00:00.010	0.000
1	22-Oct-2007 03:31:35	22-Oct-2007 03:31:35	00:00:00.010	0.000
1	22-Oct-2007 03:31:54	22-Oct-2007 03:31:54	00:00:00.010	0.000
1	22-Oct-2007 03:32:18	22-Oct-2007 03:32:18	00:00:00.010	0.000
1	22-Oct-2007 03:32:34	22-Oct-2007 03:32:34	00:00:00.010	0.000
1	22-Oct-2007 03:33:06	22-Oct-2007 03:33:06	00:00:00.010	0.000
1	22-Oct-2007 03:33:33	22-Oct-2007 03:33:33	00:00:00.010	0.000
1	22-Oct-2007 03:33:06	22-Oct-2007 03:33:06	00:00:00.010	0.000
1	22-Oct-2007 03:49:19	22-Oct-2007 03:49:19	00:00:00.010	0.000
1	22-Oct-2007 04:05:49	22-Oct-2007 04:05:49	00:00:00.010	0.000
1	22-Oct-2007 04:07:33	22-Oct-2007 04:07:33	00:00:00.010	0.000
1	22-Oct-2007 04:12:44	22-Oct-2007 04:12:44	00:00:00.010	0.000
1	22-Oct-2007 04:15:40	22-Oct-2007 04:15:40	00:00:00.010	0.000

Set	NZ02 Arrival Times	THMB Arrival Times	Difference	Offset (sec)
1	22-Oct-2007 04:53:11	22-Oct-2007 04:53:11	00:00:00.010	0.000
1	22-Oct-2007 05:13:34	22-Oct-2007 05:13:34	00:00:00.010	0.000
1	22-Oct-2007 05:19:24	22-Oct-2007 05:19:24	00:00:00.010	0.000
1	22-Oct-2007 05:25:41	22-Oct-2007 05:25:41	00:00:00.010	0.000
1	22-Oct-2007 05:35:57	22-Oct-2007 05:35:57	00:00:00.010	0.000
1	22-Oct-2007 06:02:23	22-Oct-2007 06:02:23	00:00:00.010	0.000
1	22-Oct-2007 06:03:51	22-Oct-2007 06:03:51	00:00:00.010	0.000
1	22-Oct-2007 06:08:57	22-Oct-2007 06:08:57	00:00:00.010	0.000
1	22-Oct-2007 06:12:04	22-Oct-2007 06:12:04	00:00:00.010	0.000
2	22-Oct-2007 06:24:38	22-Oct-2007 06:24:38	00:00:00.010	0.000
2	23-Oct-2007 14:51:34	23-Oct-2007 14:51:34	00:00:00.010	0.000
2	24-Oct-2007 12:57:46	24-Oct-2007 12:57:46	00:00:00.010	0.000
2	21-Oct-2007 05:20:34	21-Oct-2007 05:20:34	00:00:00.010	0.000
2	21-Oct-2007 06:05:32	21-Oct-2007 06:05:32	00:00:00.010	0.000
2	22-Oct-2007 02:52:04	22-Oct-2007 02:52:04	00:00:00.010	0.000
2	22-Oct-2007 02:56:52	22-Oct-2007 02:56:52	00:00:00.010	0.000
2	22-Oct-2007 02:58:37	22-Oct-2007 02:58:37	00:00:00.010	0.000
2	22-Oct-2007 23:24:10	22-Oct-2007 23:24:10	00:00:00.010	0.000
2	23-Oct-2007 11:30:15	23-Oct-2007 11:30:15	00:00:00.010	0.000
2	23-Oct-2007 12:27:01	23-Oct-2007 12:27:01	00:00:00.010	0.000
2	23-Oct-2007 16:53:13	23-Oct-2007 16:53:13	00:00:00.010	0.000
2	23-Oct-2007 18:09:10	23-Oct-2007 18:09:10	00:00:00.010	0.000
2	23-Oct-2007 19:44:50	23-Oct-2007 19:44:50	00:00:00.010	0.000
2	23-Oct-2007 20:03:03	23-Oct-2007 20:03:03	00:00:00.010	0.000

Set	NZ02 Arrival Times	THMB Arrival Times	Difference	Offset (sec)
2	24-Oct-2007 04:28:05	24-Oct-2007 04:28:05	00:00:00.010	0.000
2	24-Oct-2007 12:18:54	24-Oct-2007 12:18:54	00:00:00.010	0.000
2	24-Oct-2007 12:22:49	24-Oct-2007 12:22:49	00:00:00.010	0.000
2	24-Oct-2007 12:31:23	24-Oct-2007 12:31:23	00:00:00.010	0.000
2	24-Oct-2007 14:16:48	24-Oct-2007 14:16:48	00:00:00.010	0.000
2	24-Oct-2007 14:55:48	24-Oct-2007 14:55:48	00:00:00.010	0.000
2	24-Oct-2007 15:08:45	24-Oct-2007 15:08:45	00:00:00.010	0.000
2	24-Oct-2007 15:33:24	24-Oct-2007 15:33:24	00:00:00.010	0.000
2	26-Oct-2007 07:03:36	26-Oct-2007 07:03:36	00:00:00.010	0.000
2	26-Oct-2007 07:06:04	26-Oct-2007 07:06:04	00:00:00.010	0.000
2	26-Oct-2007 07:14:21	26-Oct-2007 07:14:21	00:00:00.010	0.000

Table 3: Mt. Spurr IM Relative Locations

Cluster	CRP Arrival Times	SPU Arrival Times	SPU-CRP Difference (sec)	Offset reference to 1.6674 (sec)	S-wave offset (sec)
1	27-Apr-1992 01:50:27	27-Apr-1992 01:50:28	1.6674	-0.01	0
1	08-Oct-1992 16:05:15	08-Oct-1992 16:05:16	1.6774	0	0.03
1	09-Oct-1992 07:02:31	09-Oct-1992 07:02:32	1.6674	-0.01	0.05
1	15-Oct-1992 17:14:16	15-Oct-1992 17:14:18	1.6874	0.01	0.04

Cluster	CRP Arrival Times	SPU Arrival Times	SPU-CRP Difference (sec)	Offset reference to 1.6674 (sec)	S-wave offset (sec)
1	18-Oct-1992 16:02:44	18-Oct-1992 16:02:46	1.6774	0	0.04
2	06-May-1992 13:02:47	06-May-1992 13:02:48	1.6774	0	0.00
2	06-May-1992 15:28:45	06-May-1992 15:28:47	1.6774	0	0.00
2	07-May-1992 11:10:03	07-May-1992 11:10:05	1.6874	0.01	0.00
2	08-May-1992 02:09:29	08-May-1992 02:09:31	1.6774	0	0.01
2	05-Nov-1992 20:29:14	05-Nov-1992 20:29:16	1.7273	0.0499	0.18
2	07-May-1992 03:07:08	07-May-1992 03:07:09	1.6674	-0.01	0.01
2	07-May-1992 06:44:59	07-May-1992 06:45:01	1.6674	-0.01	0.01
2	07-May-1992 15:36:23	07-May-1992 15:36:25	1.6774	0	0.01
2	08-May-1992 04:30:41	08-May-1992 04:30:42	1.6774	0	0.01
2	08-May-1992 09:18:55	08-May-1992 09:18:57	1.6774	0	0.01
2	08-May-1992 16:27:27	08-May-1992 16:27:29	1.6874	0.01	0.01
2	08-May-1992 21:54:33	08-May-1992 21:54:34	1.6774	0	0.01

Cluster	CRP Arrival Times	SPU Arrival Times	SPU-CRP Difference (sec)	Offset reference to 1.6674 (sec)	S-wave offset (sec)
2	10-May-1992 23:47:51	10-May-1992 23:47:53	1.6774	0	0.00

Table 4: Mammoth 1 IM Differences between P-wave arrival times

Set	MRD Arrival Times	MGP Arrival Times	Difference	Offset (sec)
1	29-Sep-2009 20:35:18	29-Sep-2009 20:35:19	0.9400	0
1	29-Sep-2009 20:40:44	29-Sep-2009 20:40:45	0.9400	0
1	29-Sep-2009 20:51:35	29-Sep-2009 20:51:36	0.9400	0
1	30-Sep-2009 00:48:09	30-Sep-2009 00:48:09	0.9400	0
1	30-Sep-2009 02:26:32	30-Sep-2009 02:26:33	0.9400	0
1	30-Sep-2009 01:45:07	30-Sep-2009 01:45:08	0.9400	0
1	30-Sep-2009 01:49:19	30-Sep-2009 01:49:20	0.9400	0
1	30-Sep-2009 02:04:00	30-Sep-2009 02:04:01	0.9400	0
1	30-Sep-2009 02:12:16	30-Sep-2009 02:12:17	0.9400	0
1	30-Sep-2009 02:20:40	30-Sep-2009 02:20:41	0.9400	0
1	30-Sep-2009 02:24:48	30-Sep-2009 02:24:49	0.9400	0
1	30-Sep-2009 03:16:23	30-Sep-2009 03:16:24	0.9400	0
1	30-Sep-2009 03:20:27	30-Sep-2009 03:20:28	0.9400	0
1	30-Sep-2009 03:23:01	30-Sep-2009 03:23:02	0.9400	0
1	30-Sep-2009 03:51:21	30-Sep-2009 03:51:22	0.9400	0

Set	MRD Arrival Times	MGP Arrival Times	Difference	Offset (sec)
1	30-Sep-2009 03:54:03	30-Sep-2009 03:54:04	0.9400	0
1	30-Sep-2009 03:59:38	30-Sep-2009 03:59:39	0.9400	0
1	30-Sep-2009 04:07:41	30-Sep-2009 04:07:42	0.9400	0
1	30-Sep-2009 04:23:36	30-Sep-2009 04:23:37	0.9400	0
1	30-Sep-2009 04:36:28	30-Sep-2009 04:36:29	0.9400	0
1	30-Sep-2009 04:48:33	30-Sep-2009 04:48:34	0.9400	0
1	30-Sep-2009 05:06:39	30-Sep-2009 05:06:40	0.9400	0
1	30-Sep-2009 05:46:06	30-Sep-2009 05:46:06	0.9400	0
1	30-Sep-2009 03:33:30	30-Sep-2009 03:33:31	0.9400	0
2	29-Sep-2009 19:18:57	29-Sep-2009 19:18:58	0.9400	0
2	29-Sep-2009 19:30:39	29-Sep-2009 19:30:40	0.9400	0
2	29-Sep-2009 20:46:36	29-Sep-2009 20:46:37	0.9400	0
2	29-Sep-2009 21:50:36	29-Sep-2009 21:50:37	0.9400	0
2	29-Sep-2009 23:58:32	29-Sep-2009 23:58:33	0.9400	0
2	29-Sep-2009 21:54:37	29-Sep-2009 21:54:38	0.9400	0
2	30-Sep-2009 02:51:24	30-Sep-2009 02:51:25	0.9400	0
2	30-Sep-2009 04:02:53	30-Sep-2009 04:02:54	0.9400	0
2	30-Sep-2009 04:47:07	30-Sep-2009 04:47:08	0.9400	0
2	30-Sep-2009 05:09:27	30-Sep-2009 05:09:28	0.9400	0
2	30-Sep-2009 05:22:47	30-Sep-2009 05:22:48	0.9400	0
2	30-Sep-2009 05:29:29	30-Sep-2009 05:29:30	0.9400	0

Table 5: Mammoth 2 IM Differences between P-wave arrival times

Set	MRD Arrival Times	MGP Arrival Times	Difference	Offset (sec)
1	29-Sep-2009 19:16:49	29-Sep-2009 19:16:55	5.9000	0
1	29-Sep-2009 21:05:40	29-Sep-2009 21:05:46	5.9000	0
1	29-Sep-2009 21:43:17	29-Sep-2009 21:43:23	5.9000	0
1	29-Sep-2009 22:04:55	29-Sep-2009 22:05:01	5.9000	0
1	29-Sep-2009 22:23:22	29-Sep-2009 22:23:28	5.9000	0
1	29-Sep-2009 22:30:16	29-Sep-2009 22:30:22	5.9000	0
1	30-Sep-2009 00:39:03	30-Sep-2009 00:39:09	5.9000	0
2	29-Sep-2009 18:19:09	29-Sep-2009 18:19:15	5.9000	0
2	29-Sep-2009 18:21:23	29-Sep-2009 18:21:29	5.9000	0
2	29-Sep-2009 18:39:24	29-Sep-2009 18:39:30	5.9000	0
2	29-Sep-2009 19:04:14	29-Sep-2009 19:04:19	5.9000	0
2	29-Sep-2009 19:50:53	29-Sep-2009 19:50:59	5.9000	0
2	29-Sep-2009 15:14:21	29-Sep-2009 15:14:27	5.9000	0
2	29-Sep-2009 15:32:17	29-Sep-2009 15:32:23	5.9000	0
2	29-Sep-2009 15:36:00	29-Sep-2009 15:36:06	5.9000	0
2	29-Sep-2009 15:44:46	29-Sep-2009 15:44:52	5.9000	0
2	29-Sep-2009 15:49:37	29-Sep-2009 15:49:43	5.9000	0
2	29-Sep-2009 16:05:39	29-Sep-2009 16:05:45	5.9000	0
2	29-Sep-2009 18:59:25	29-Sep-2009 18:59:31	5.9000	0

Table 6: Synthetic Waveform Correlation Coefficients

Scenario	Correlation Coefficient **Whole waveform**	Correlation Coefficient **P-wave** (0.25 secs)	Correlation Coefficient **S-wave** (0.9 secs)	Figure
Opposite Motion				
Reverse vs normal 45° dip - all stations	-1	-1	-1	25
Strike slip RL vs LL - all stations	-1	-1	-1	26
Different Strikes				
RL SS 20° vs 40° strike	-1 on stations between strikes. 1 on all other stations	-1 on stations between strikes. 1 on all other stations	-1 on stations between strikes. 1 on all other stations	
Note: Bouch program in Seisan does not account for changes in amplitude due to differences in azimuth of the station recording the event. Correlation coefficients for this experiment are therefore artificially high.				
Different Dips (azimuths are for station locations) - strike = 0°				
Thrust 15° vs 80° dip	30° azimuth: 0.24 60° azimuth: 0.24 210° azimuth: -0.23 240° azimuth: 0.30	30° azimuth: 0.69 60° azimuth: 0.48 210° azimuth: -0.34 240° azimuth: 0.67	30° azimuth: 0.25 60° azimuth: 0.35 210° azimuth: -0.28 240° azimuth: -0.30	27
Thrust 15° vs 45° dip	30° azimuth: 0.23 120° azimuth: 0.22 210° azimuth: 0.32 240° azimuth: 0.30	30° azimuth: 0.60 120° azimuth: 0.58 210° azimuth: 0.47 240° azimuth: 0.46	30° azimuth: 0.34 120° azimuth: 0.28 210° azimuth: 0.34 240° azimuth: 0.32	
Thrust 45° vs 80° dip	30° azimuth: 0.22 240° azimuth: -0.27	30° azimuth: 0.55 240° azimuth: 0.73	30° azimuth: 0.25 240° azimuth: -0.38	
Different Depths				
Thrust at 14.1km depth vs normal at 15km depth	0.34	-0.70	-0.39	

Scenario	Correlation Coefficient Whole waveform	Correlation Coefficient **P-wave** (0.25 secs)	Correlation Coefficient **S-wave** (0.9 secs)	Figure
Thrusts at 14.1km depth vs at 15km depth	-0.34	0.70	0.39	
Thrust at 14km vs thrust at 14.1 km	0.80	0.94	0.85	
Thrust at 14km vs thrust at 15km	-0.34	0.56	-0.35	28

Notes:
Earthquakes at 5 km depth and stations 5 km from epicenter unless otherwise noted

Table 7: IM Analysis Results

IM	Colocated	Temporal Overlap	Amplitude Ratios	Inversion in all stations	Likely Mechanism
Nechako 1 Clusters 1/3	Y	N	Same	Y	Dike motion between fractures
Nechako 1 Clusters 2/3	Y	Y	Different	Y	Different strike
Nechako 2	Y	Y	Same	Y	Dike motion between fractures
Spurr	N	N	NM	N	Dike Inflation
Mammoth 1	Y	Y	NM	Y	Different strike
Mammoth 2	Y	Y	NM	Y	Different strike

Note:
NM Not Measured

FIGURES

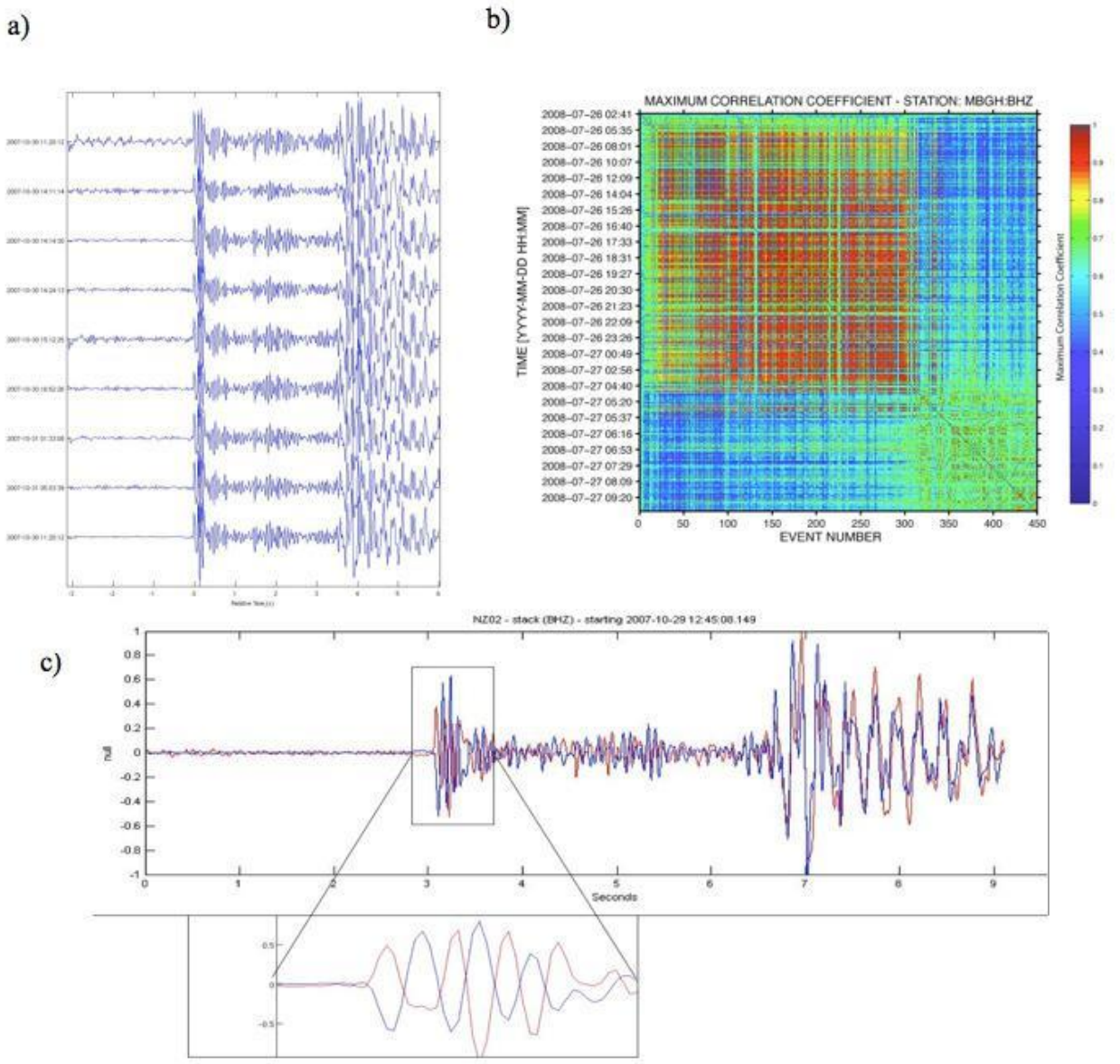

Fig. 1. a) A group of similar waveforms interpreted to be a multiplet. b) Cross-correlation diagram. Events are plotted on both the x- and y-axis and color represents the correlation coefficient. Notice there are only positive coefficients. c) A reversing multiplet. Shown are two stacks of earthquakes from the Nechako Basin earthquake swarm of 2007. In red is a stack of a second cluster in that multiplet, showing the inverted nature of the P-wave. In blue is a stack of a multiplet that is the inverse of the red stack in the P-wave. Notice that in the S-waves, they are no longer inverted.

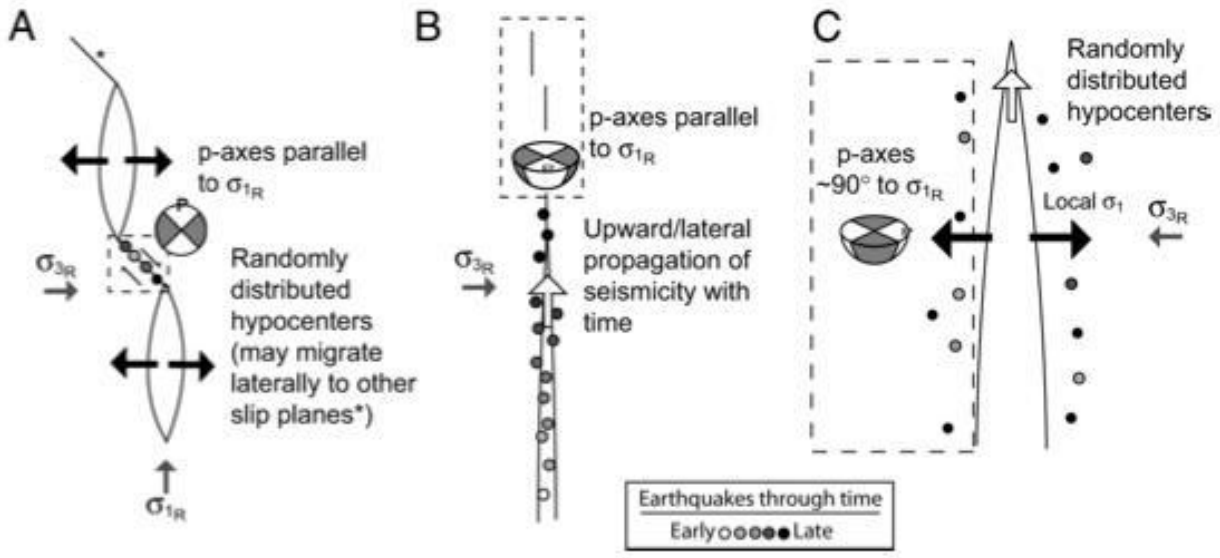

Fig. 2. Three-part model of dike-induced earthquakes and their associated focal mechanisms. A) Earthquakes occurring between en echelon segments of dikes. B) Earthquakes occurring at the tip of a propagating dike. C) Earthquakes occurring around the walls of an expanding dike with P-axes ~90° to the regional P-axis. This shift in the P-axes changes the focal mechanism and can cause IMs. Taken from Roman et al. (2006).

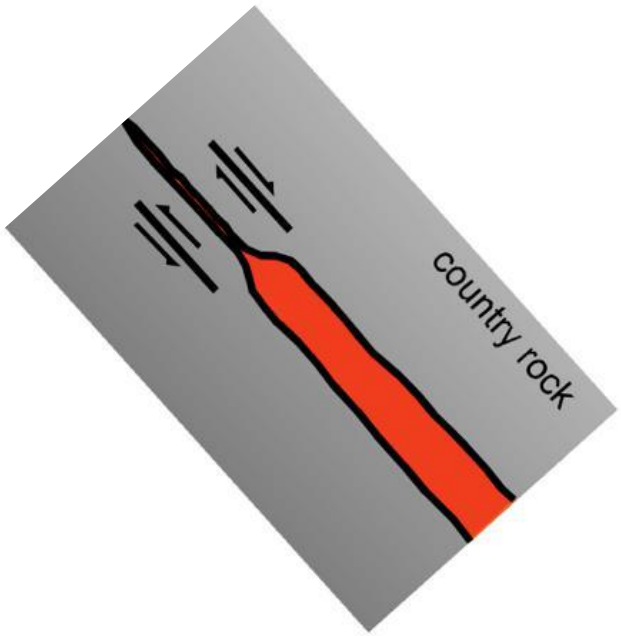

Fig. 3. Parallel fractures on either side of a dike tip cause opposite senses of motion. These would generate closely-located earthquakes with inverted mechanisms. Figure modified from White et al. (2011).

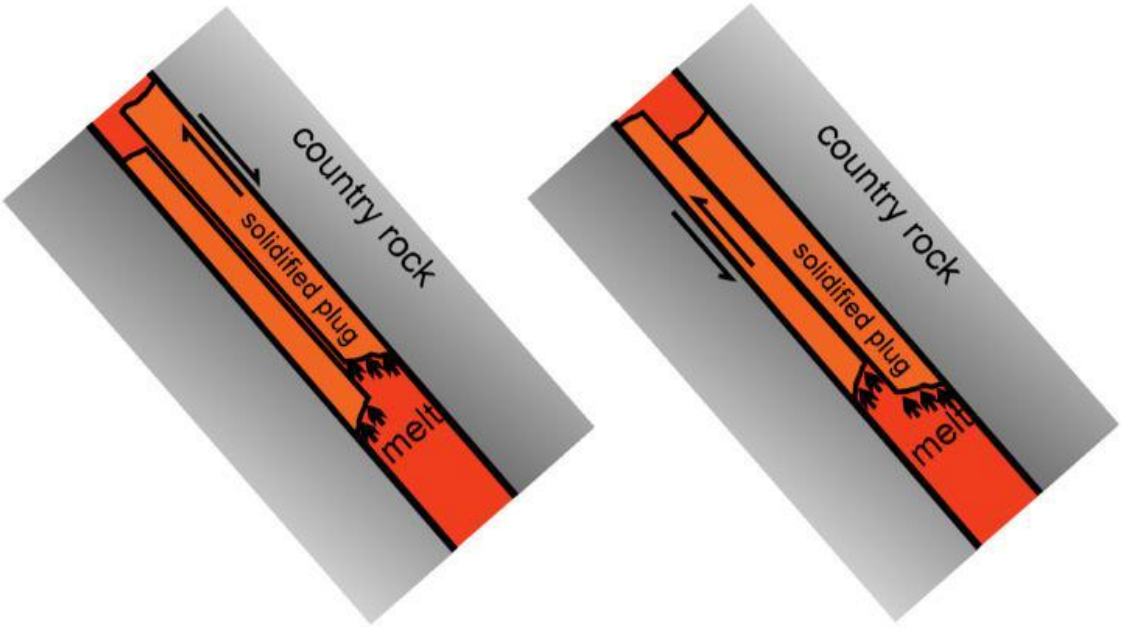

Fig. 4. Opposite fault motions caused by slip of either side of a solidified plug in a dipping dike. As with the case in Figure 3, earthquakes generated on opposite sides of the dike would have different senses of motion despite their proximity. Taken from White et al. (2011).

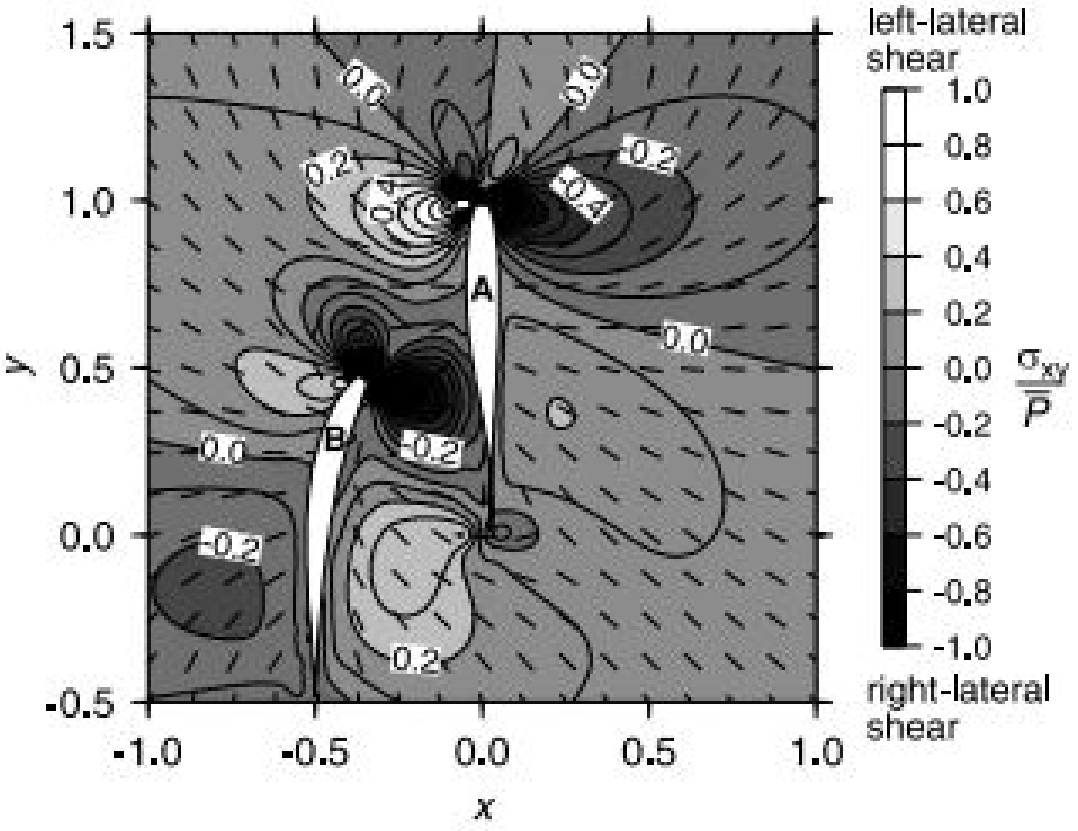

Fig. 5. Shear stresses (σ_{xy} normalized by the average driving pressure P) predicted by a 2-D numerical model of two dikes of equal buoyancy and length (A and B). A is an earlier dike intrusion that changed the local stress field to force dike B to turn towards it. Left lateral shear is shown to the left of the tip of dike A and right lateral shear is shown directly below it at the tip of dike B. The third mechanism proposed by White et al. (2011) predicts opposite fault motions occurring in these two places and the fourth mechanism predicts opposite motions on fractures between the two dikes or dike segments. Figure taken from Ito and Martel (2002).

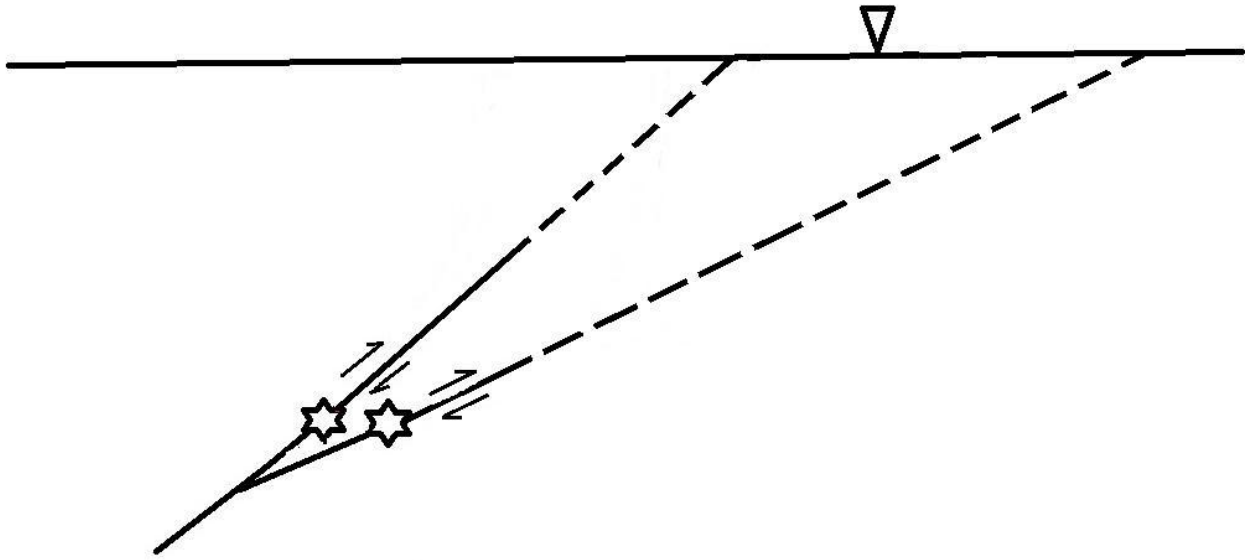

Fig. 6. Two adjacent earthquakes (stars) on faults with slightly different strikes put a seismometer (triangle) in two different quadrants. The earthquake on the left puts the seismometer in a dilatational quadrant and the earthquake on the right puts the seismometer in a compressional quadrant.

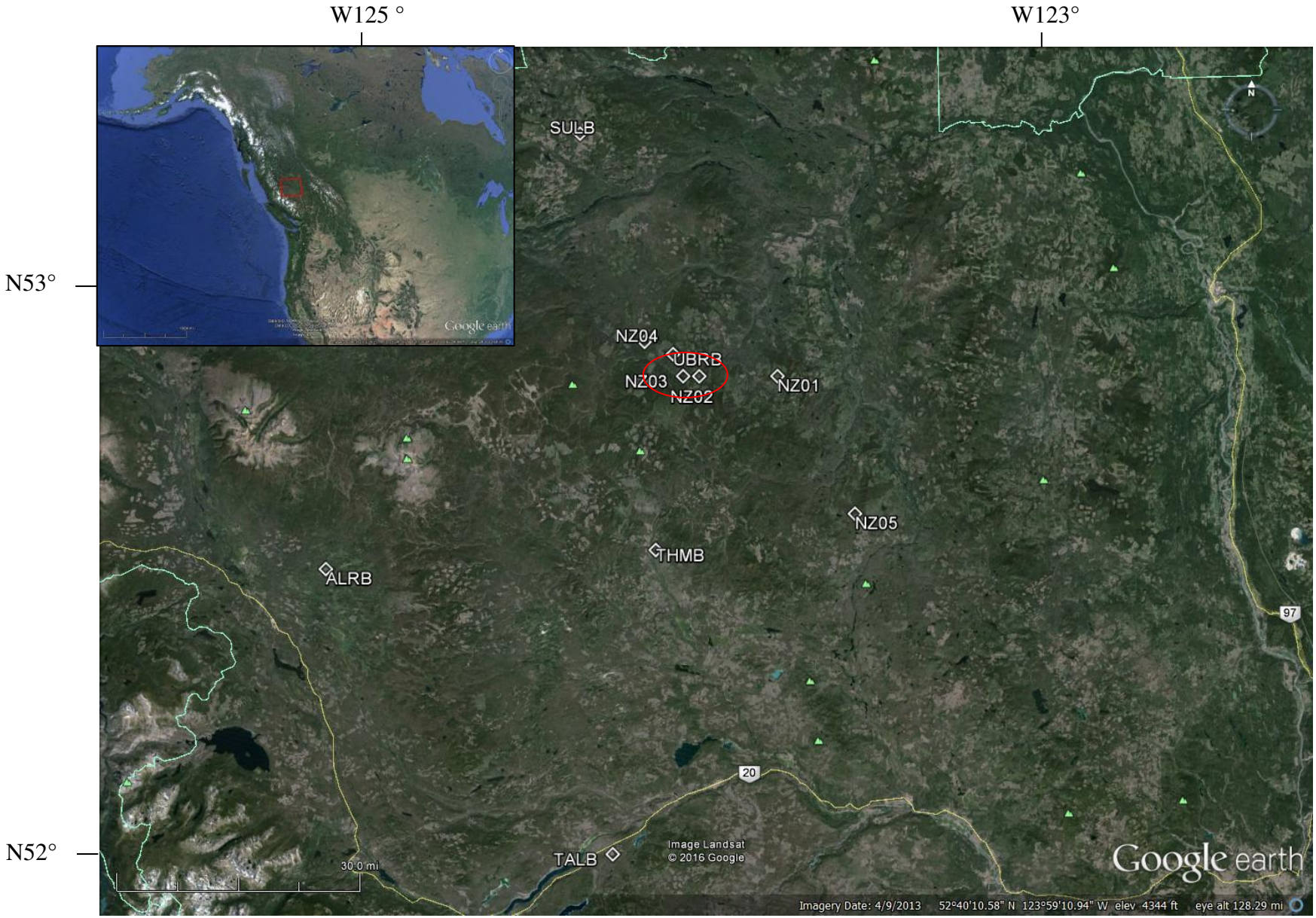

Fig. 7. Map of seismic network around the Nechako earthquake swarm. The red circle shows the approximate epicenter of the earthquake swarm.

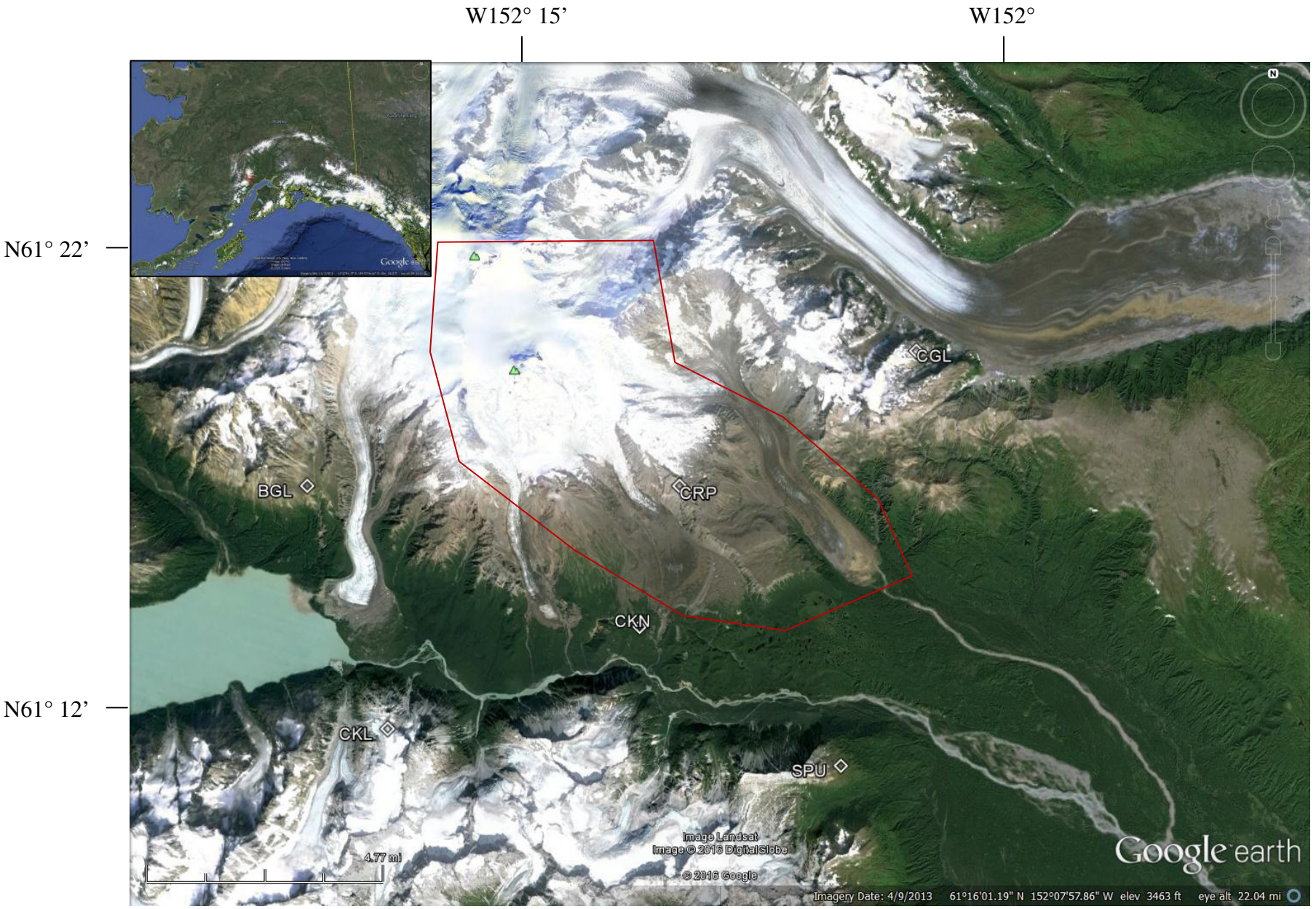

Fig. 8. Map of the seismic network surrounding Mt. Spurr. The red polygon shows the approximate epicenter of the earthquake swarm. Diamonds represent seismometers used in this study.

Fig. 9. Map of the seismic network surrounding Mammoth Mountain. Diamonds represent seismometers used in this study. The red circle shows the approximate epicenter of the earthquake swarm.

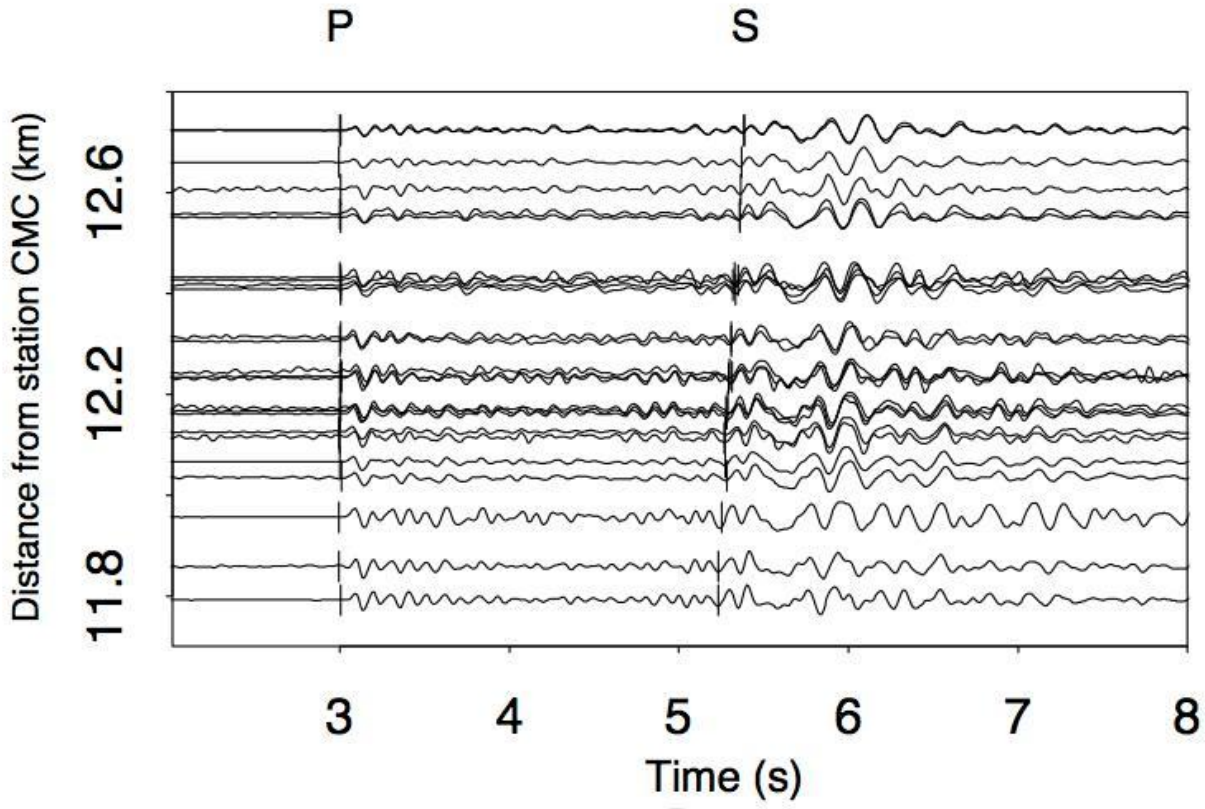

Fig. 10. Waveforms lined up according to the P-wave arrival times. Lining up the waveforms according to S-waves and measuring the amount of shift gives the S-wave offset value. Figure from Waldhauser et al. (1999).

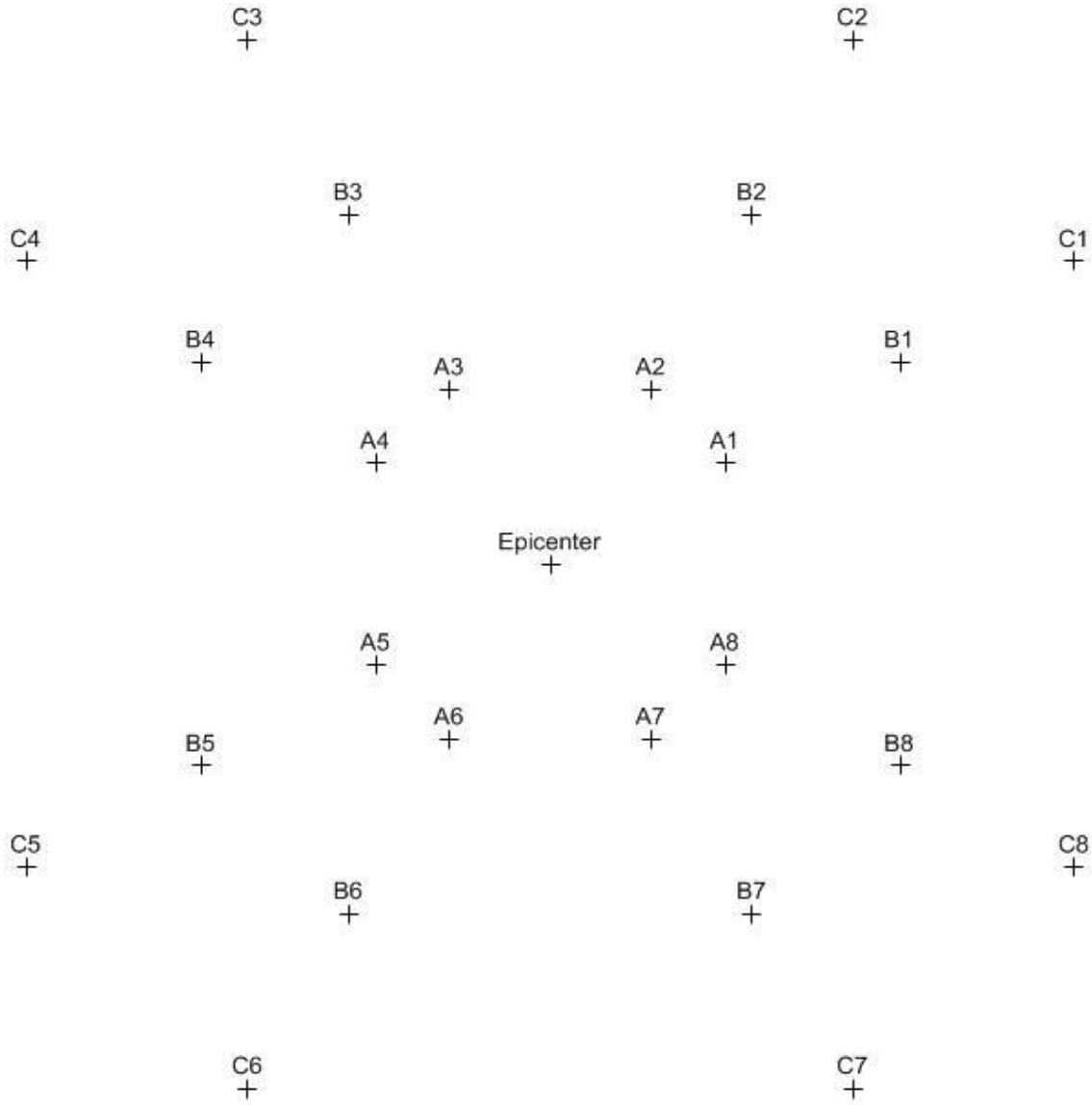

Fig. 11. Map view of synthetic seismic array. Stations starting with “A”, “B”, and “C” are 5 km, 10 km, and 15 km from the epicenter respectively.

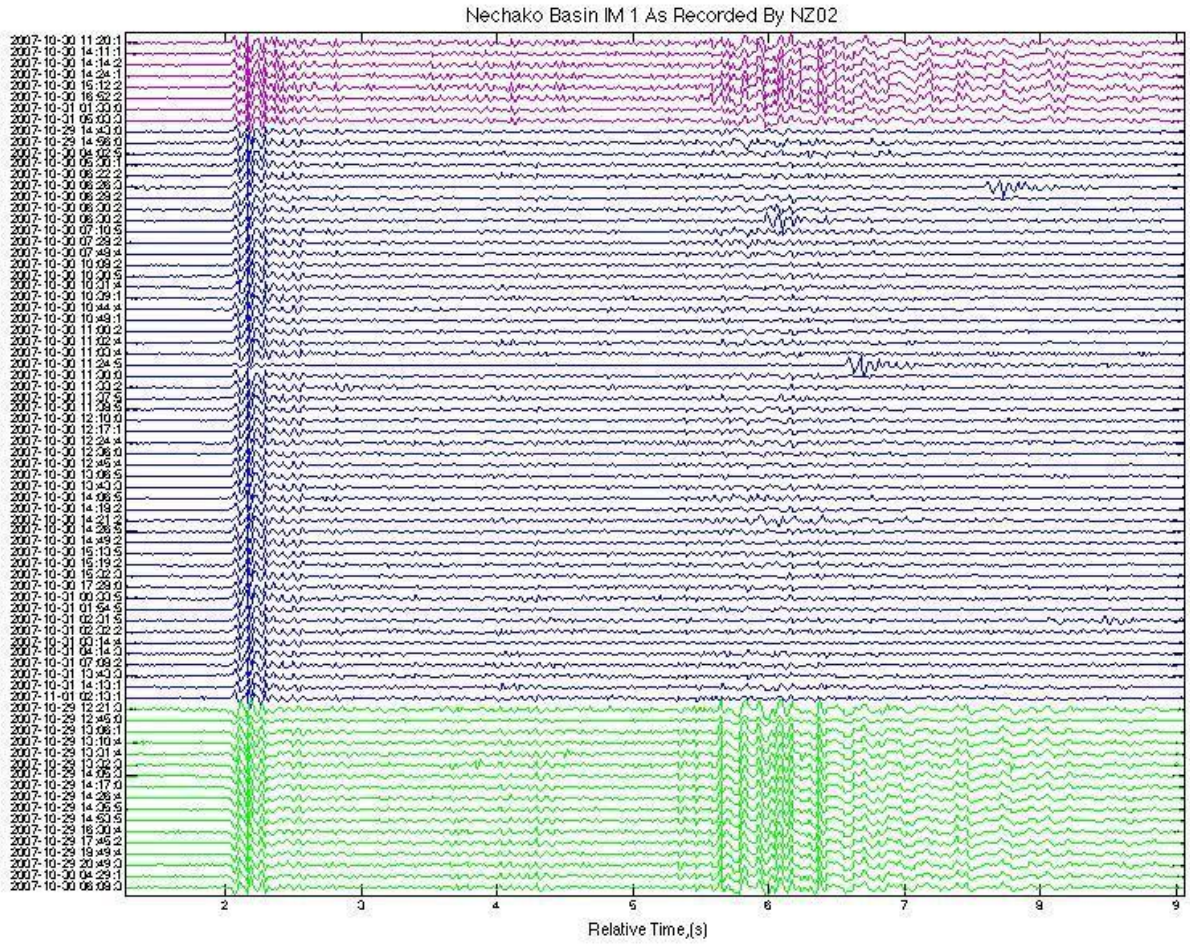

Fig. 12. Seismic recordings of Nechako 1 as recorded by NZ02. Cluster 1 is in magenta, cluster 2 is blue, and cluster 3 is green. Clusters 1 and 2 have similar P-waves, which are inverted to cluster 3's P-waves. Clusters 1 and 3 have similar S-waves, while cluster 2 has almost none.

a)

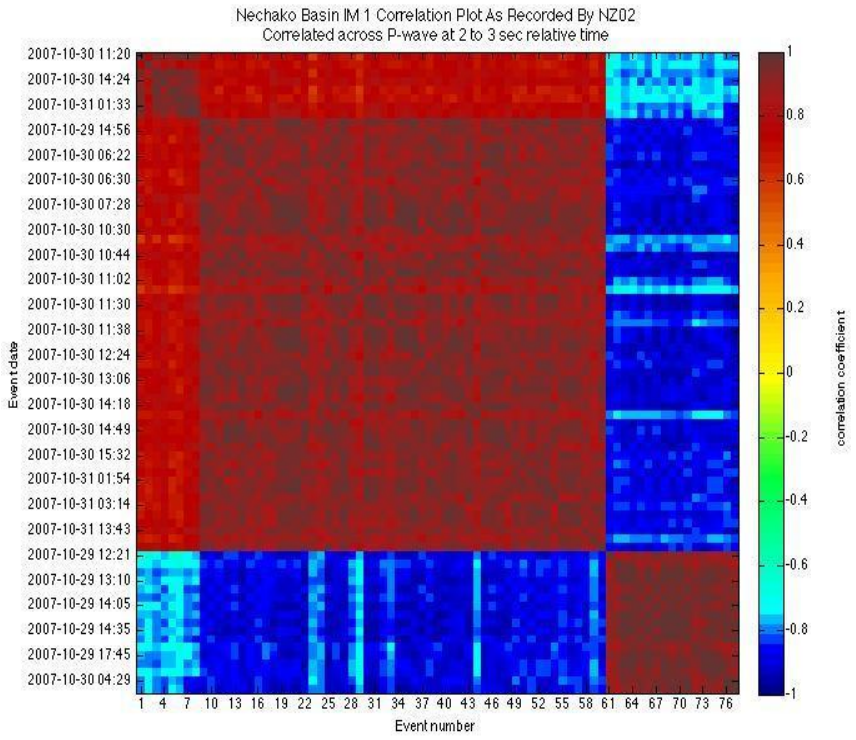

b)

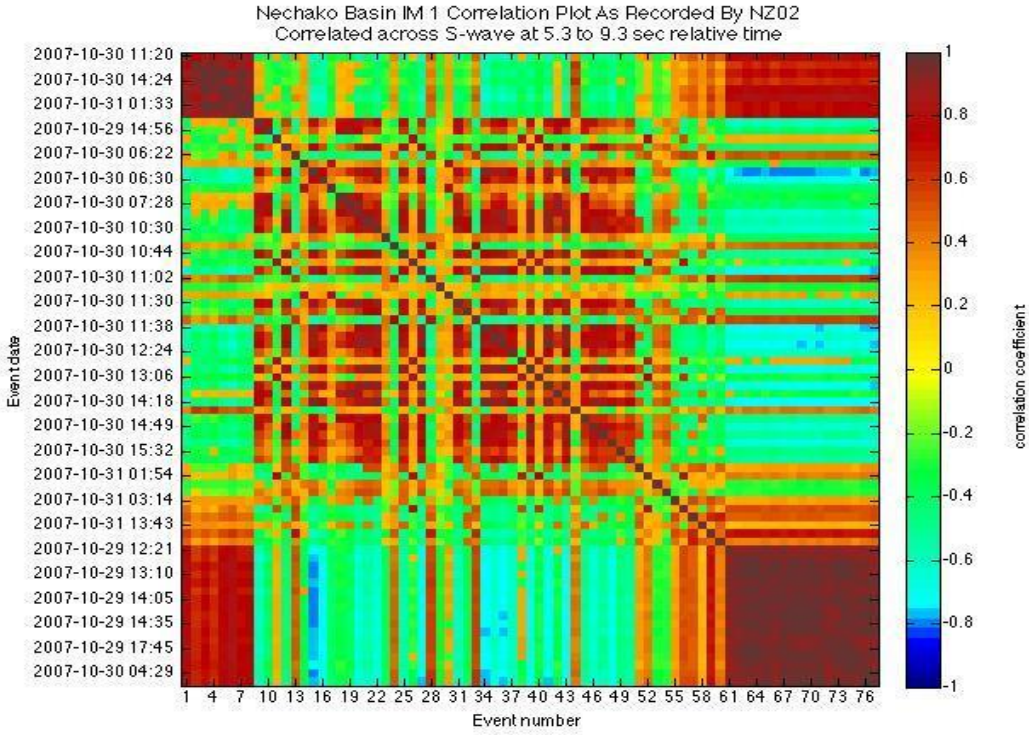

Fig. 13. Correlograms of Nechako 1 as recorded by NZ02. a) P-wave correlations and b) S-wave correlations. P-waves are highly correlated in clusters 1 and 2 as shown in red and negatively correlated in cluster 3 as shown in blue. S-waves are highly correlated in clusters 1 and 3 as shown in red and weakly correlated with cluster 2 as shown by greens and oranges.

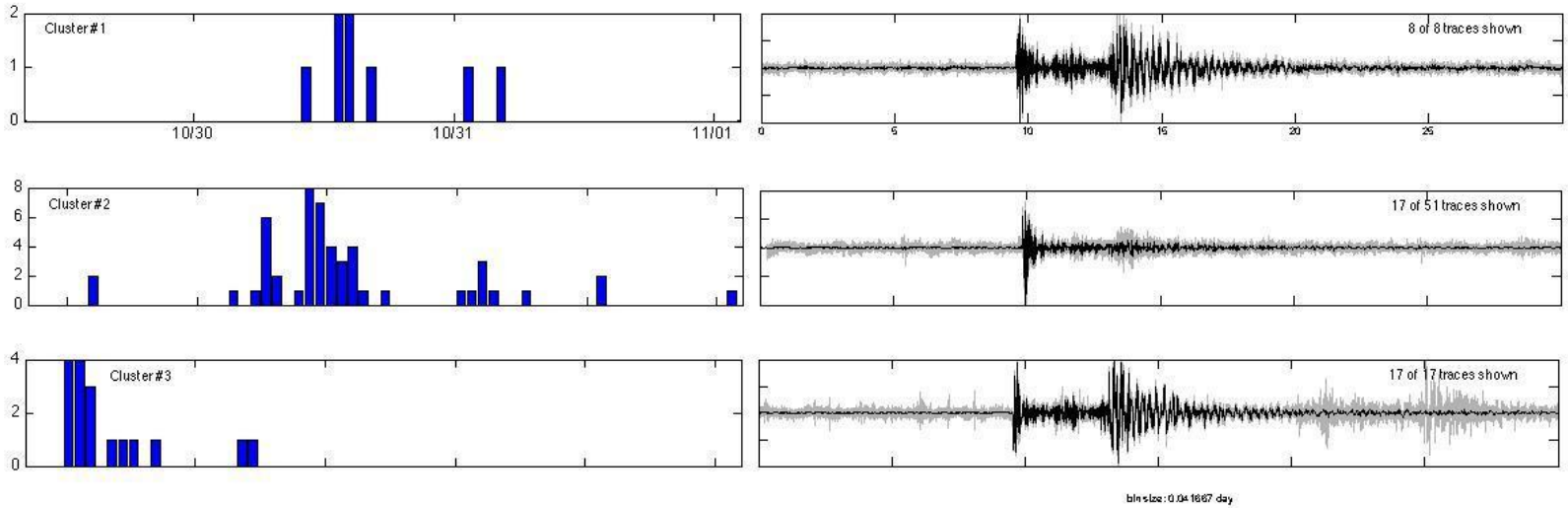

Fig. 14. Occurrence plot of the three clusters of Nechako 1. Cluster 3 occurs first, then cluster 1 occurs. Cluster 2 occurred contemporaneously with the other two (but mostly after cluster 3).

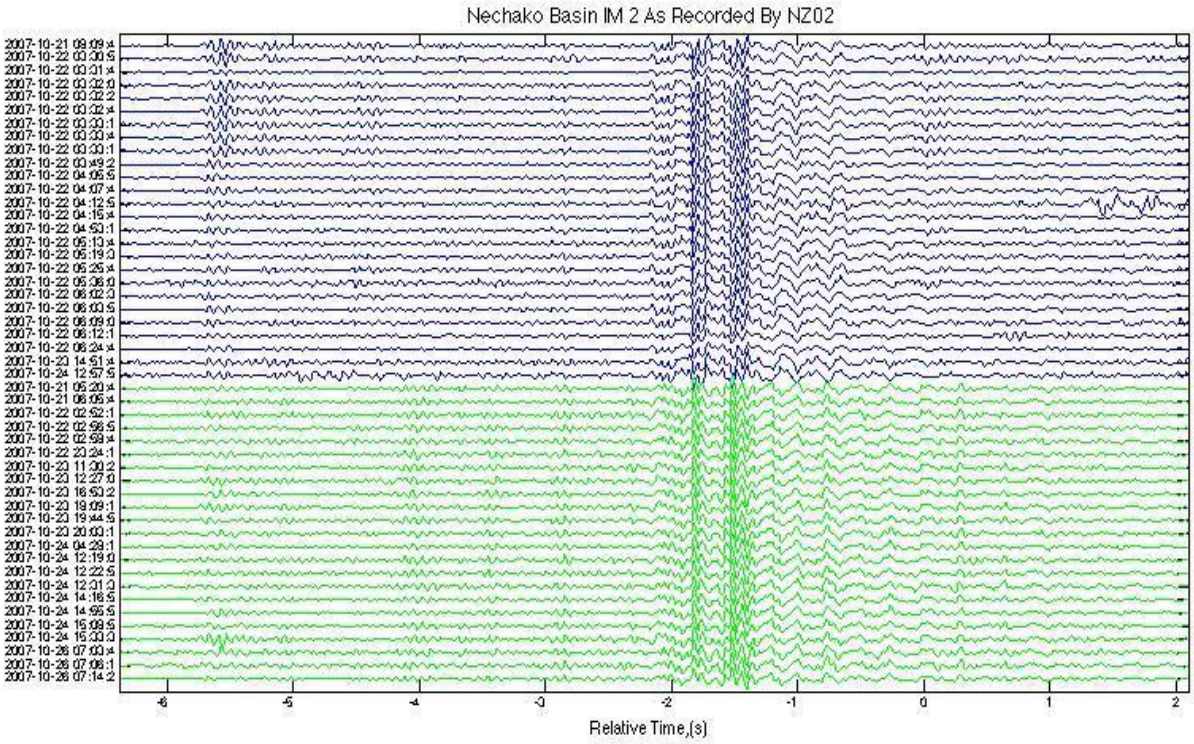

Fig. 15. Seismic recordings of Nechako 2 as recorded by NZ02, aligned by cross-correlation. Cluster 1, shown in blue, includes 23 earthquakes and cluster 2, shown in green, includes 26.

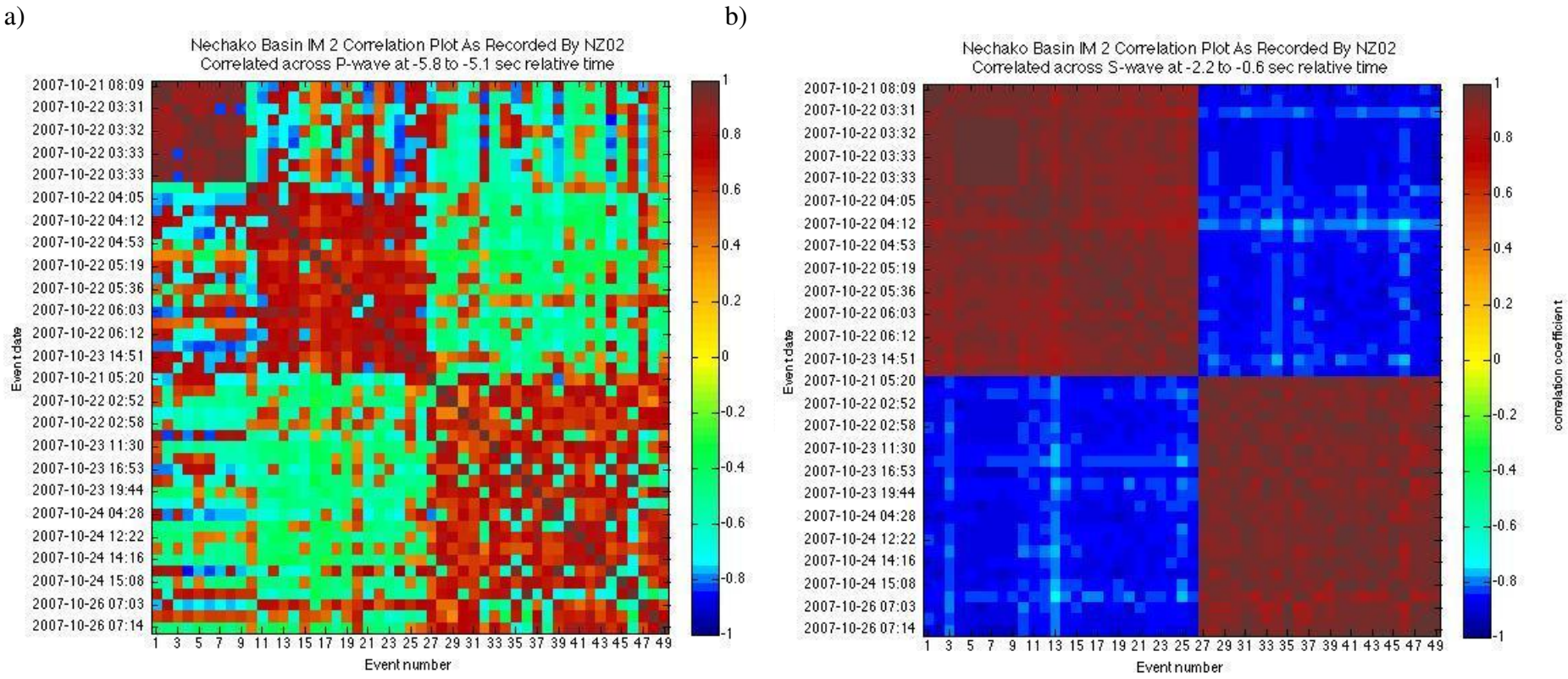

Fig. 16. Correlograms of Nechako 2 as recorded by NZ02. a) P-wave correlations and b) S-wave correlations. Weak correlations are shown in the P-waves and very strong correlations are shown in the S-waves.

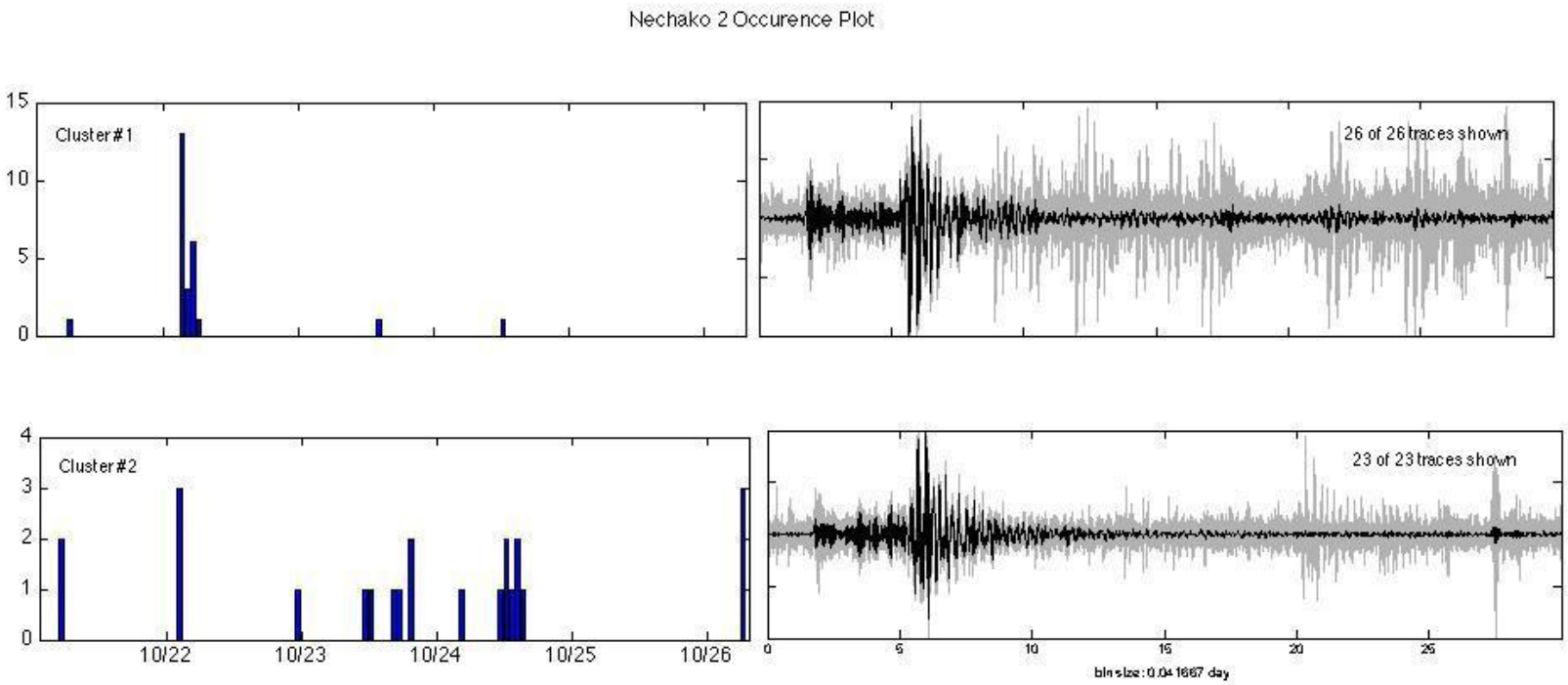

Fig. 17. Occurrence plot of Nechako 2. The two clusters occurred contemporaneously with most of cluster 1 occurring on October 22nd. Cluster 2 is more spread out over four days.

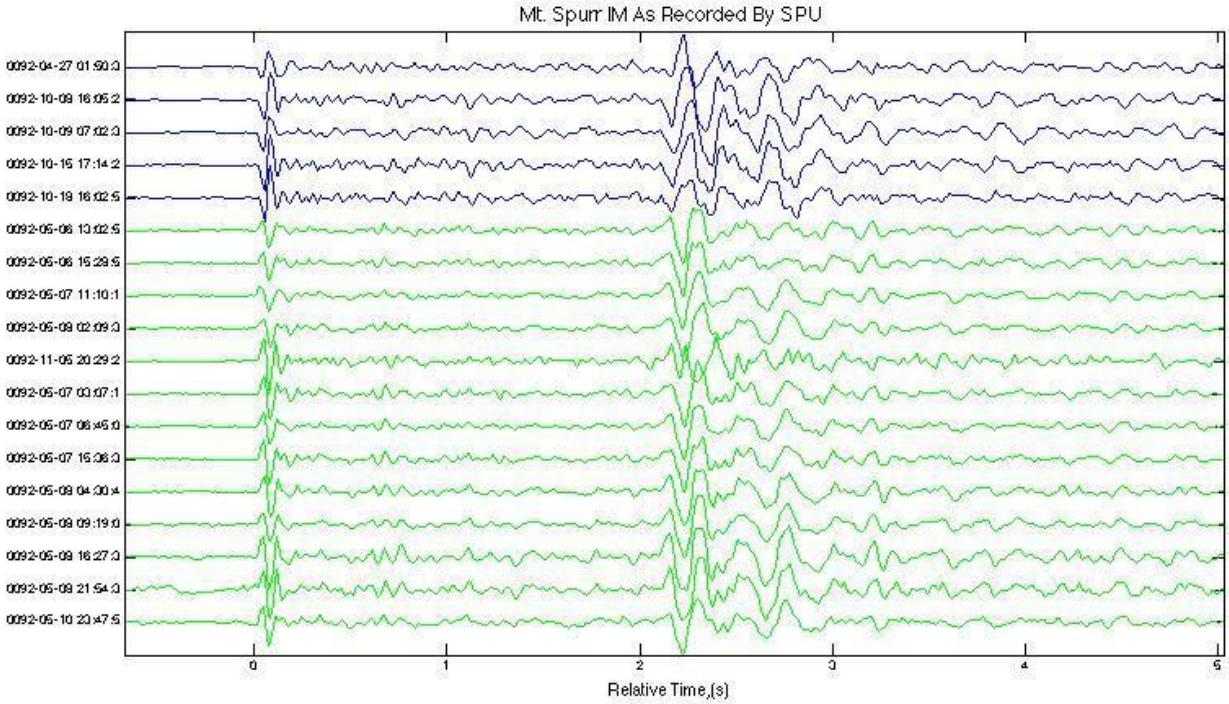

Fig. 18. Seismic recordings of Mt. Spurr IM as recorded by SPU, aligned by cross-correlation. Cluster 1, shown in blue, includes five earthquakes and cluster 2, shown in green, includes 13.

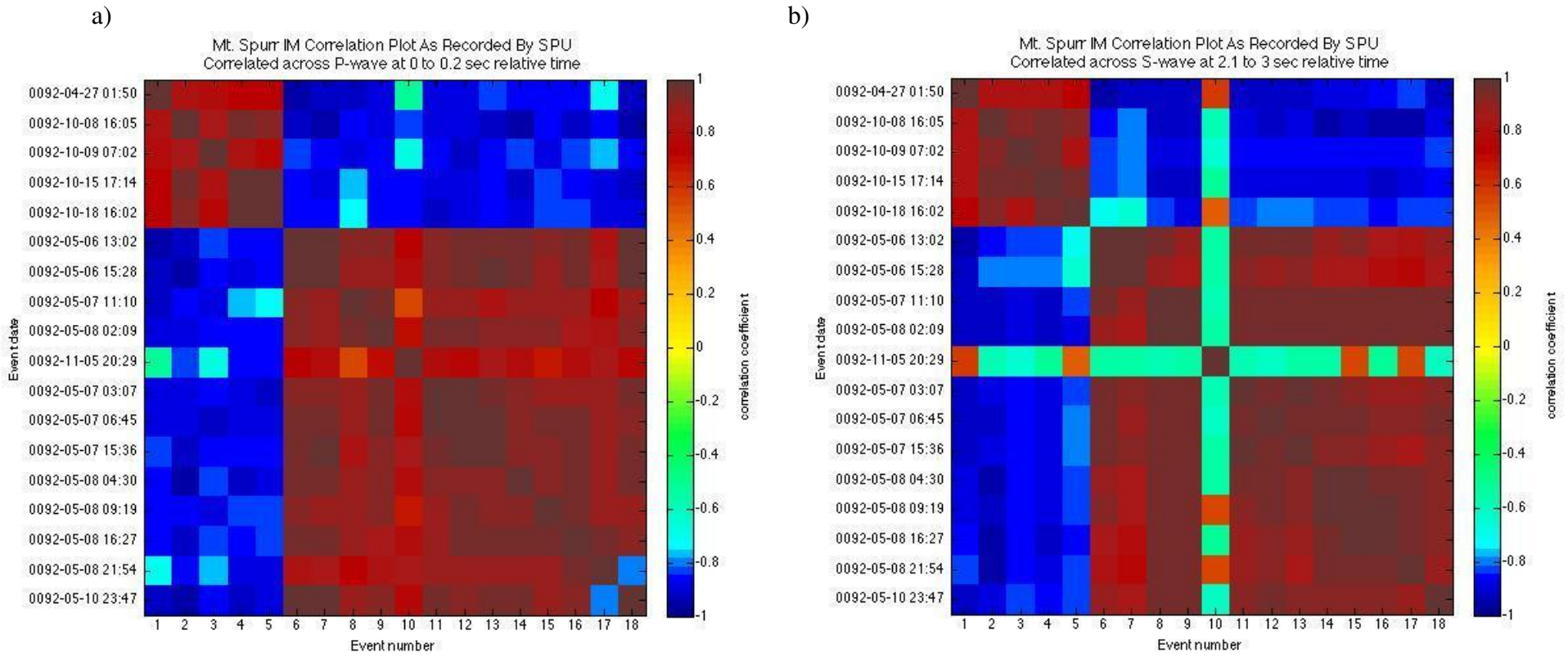

Fig. 19. Correlograms of Spurr IM. a) P-wave correlations and b) S-wave correlations. Strong correlations are shown in P- and S-waves as red for positive correlations and blue for negative correlations.

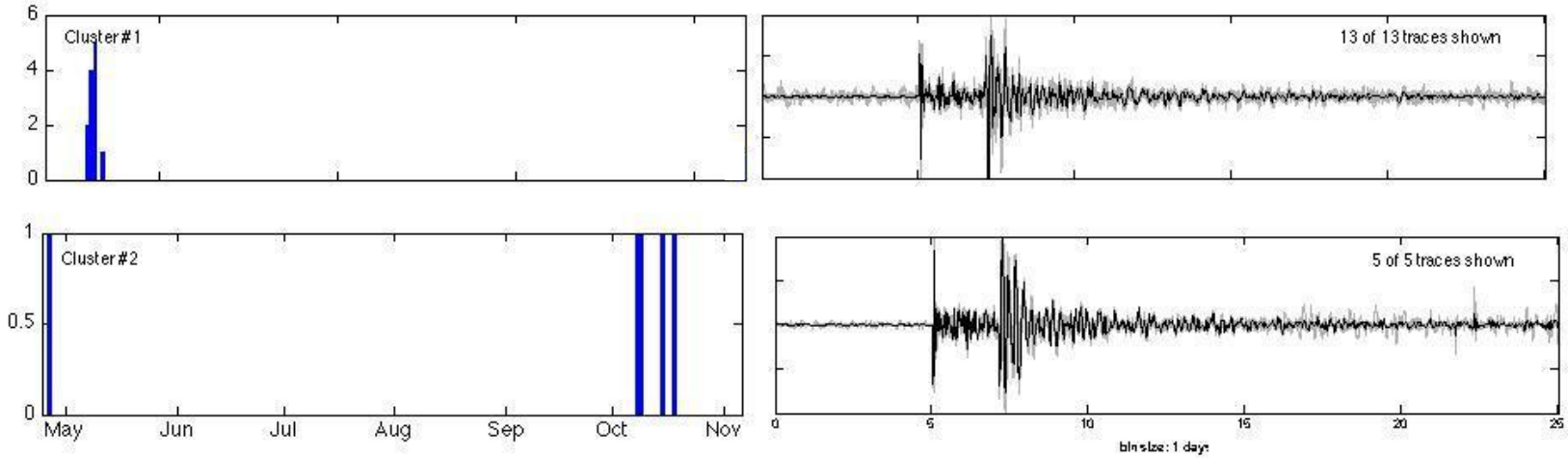

Fig. 20. Occurrence plot of Spurr IM. One event from cluster 2 occurred, then cluster 1, then the rest of cluster 2. The event shown in November was dropped from the analysis because of low correlation to the others.

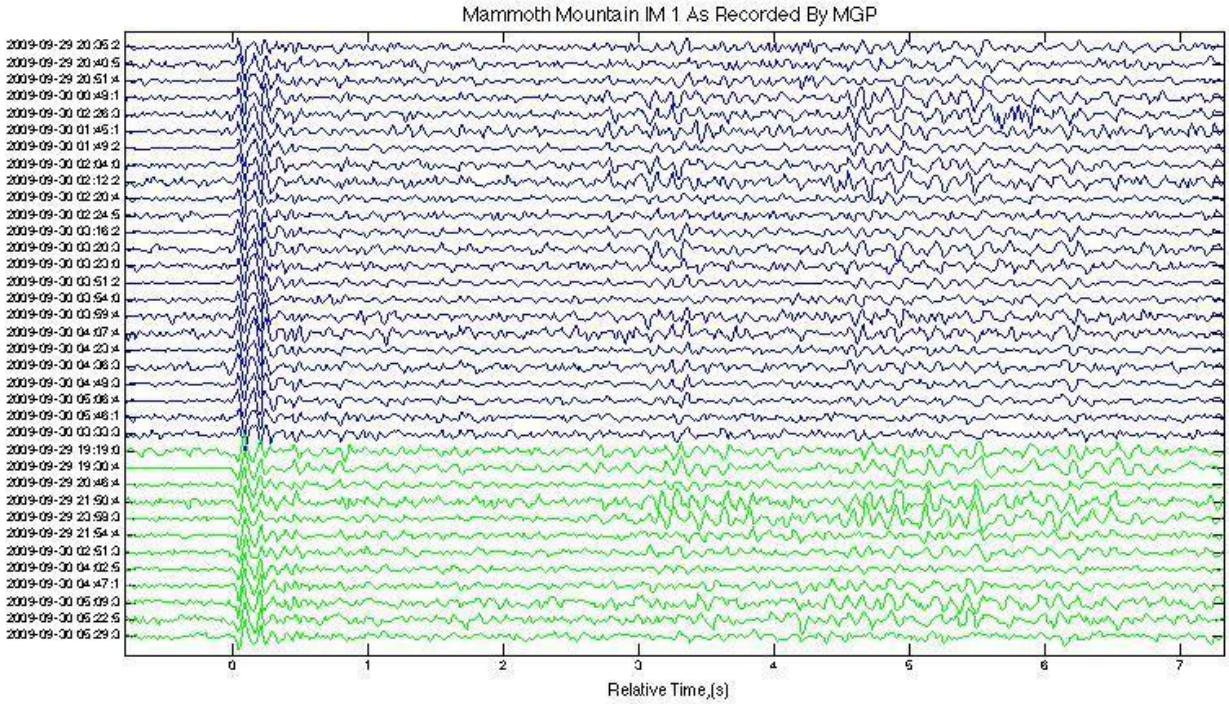

Fig. 21. Seismic recordings of Mammoth IM 1 as recorded by MGP. Cluster 1, shown in blue, has 24 earthquakes and cluster 2, shown in green, has 12.

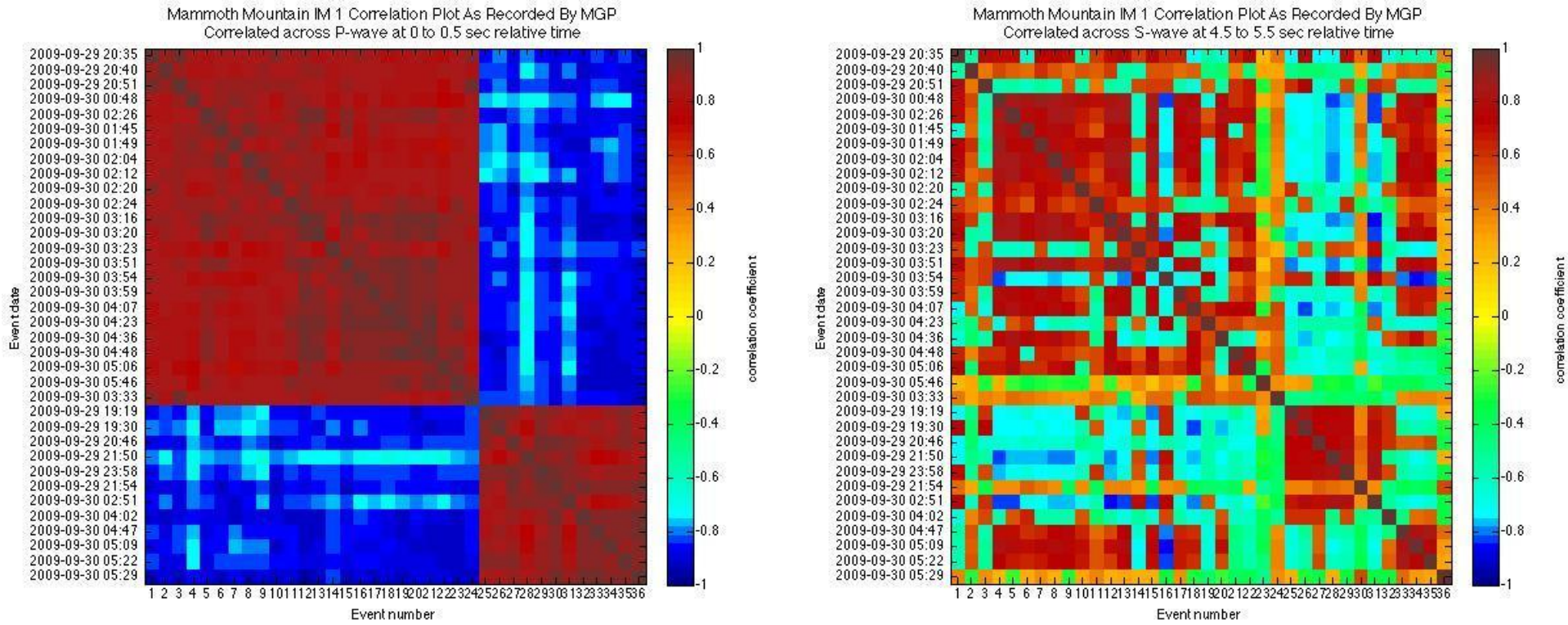

Fig. 22. Correlograms of Mammoth IM 1. a) shows P-wave correlations and b) shows S-wave correlations. The dark reds and blues show strong positive and negative correlations in the P-waves. No definitive correlations are shown in the S-waves.

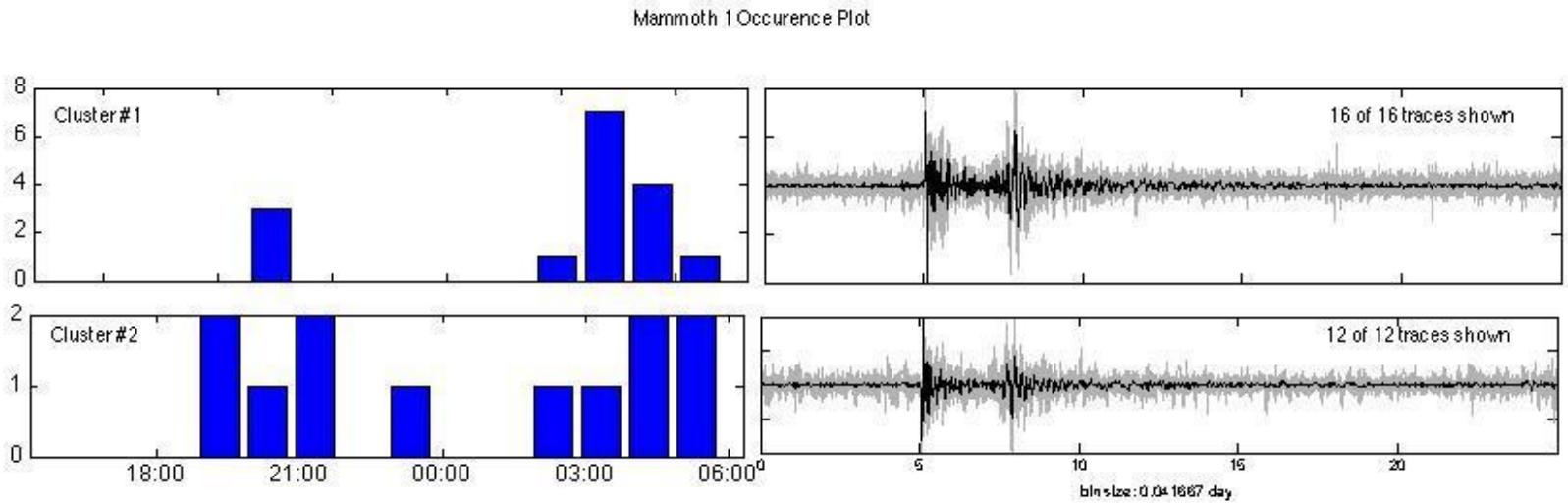

Fig. 23. Occurrence plot of Mammoth IM 1. Both clusters occurred contemporaneously.

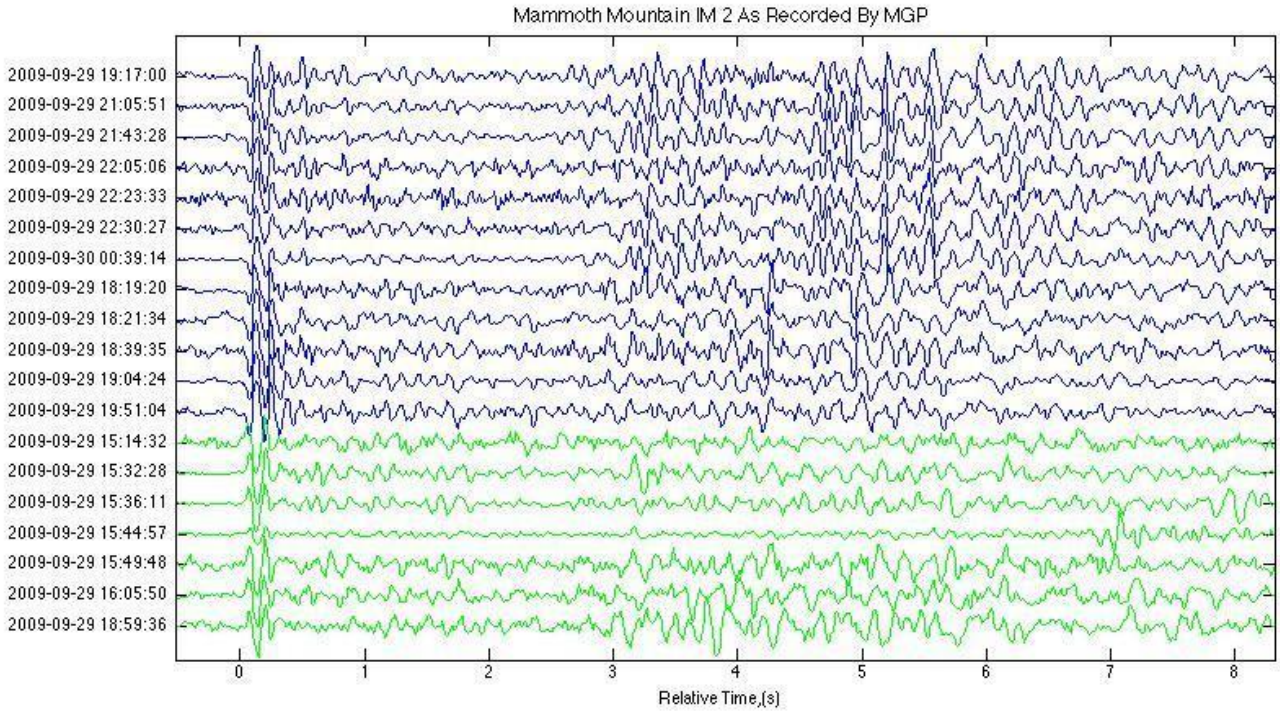

Fig. 24. Seismic recordings of Mammoth IM 2 as recorded by MGP. Cluster 1, shown in blue, includes seven earthquakes and cluster 2, shown in green, includes 12.

a)

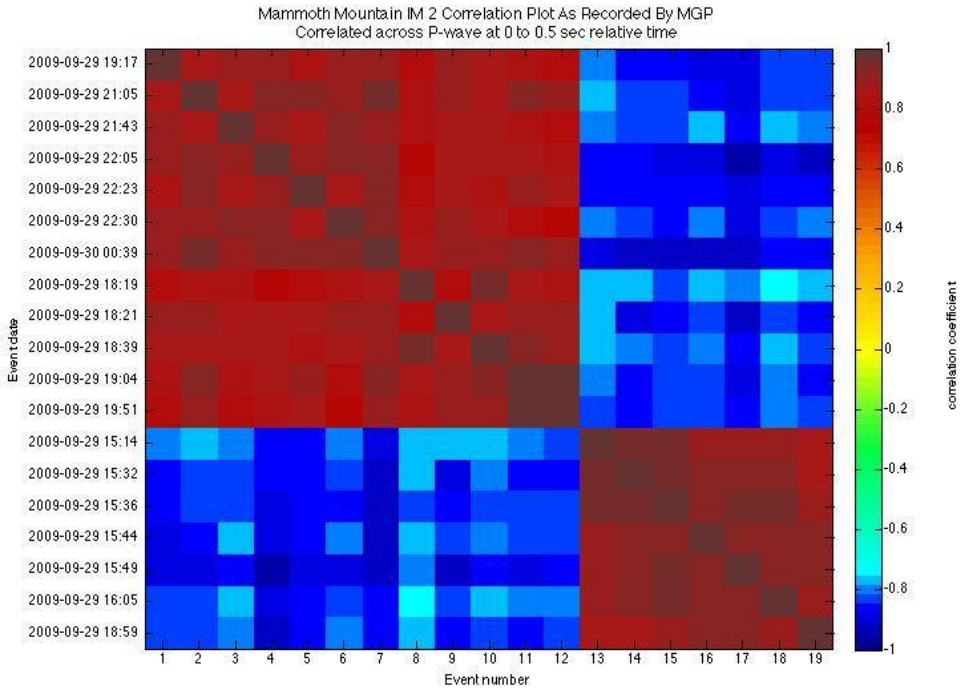

b)

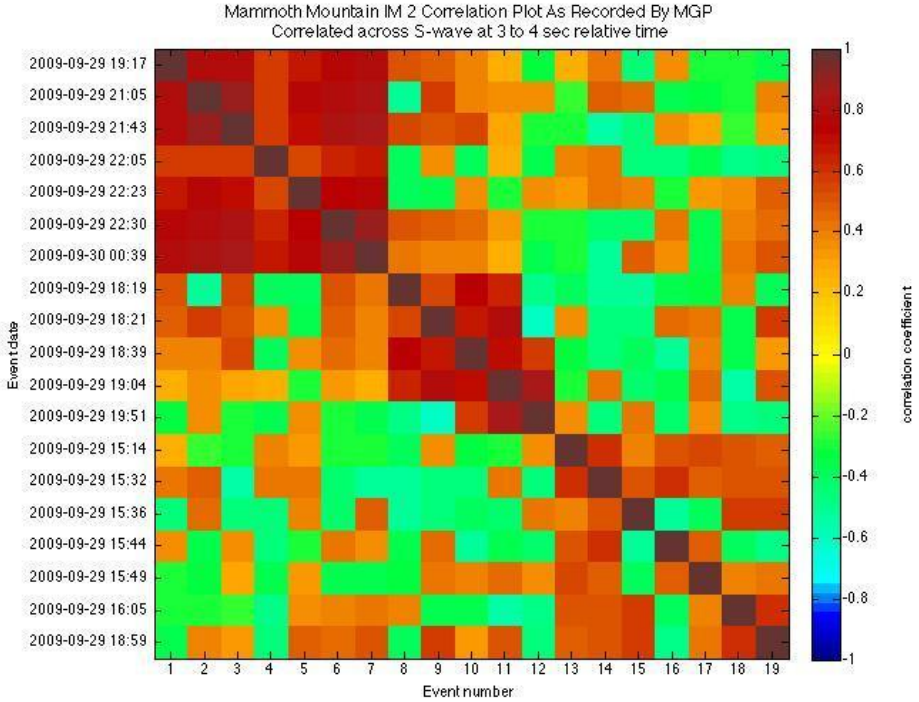

Fig. 25. Correlograms of Mammoth IM 2. a) shows P-wave correlations and b) shows S-wave correlations. Dark reds and blues represent strong positive and negative correlations in the P-waves. No definitive correlations are shown in the S-waves.

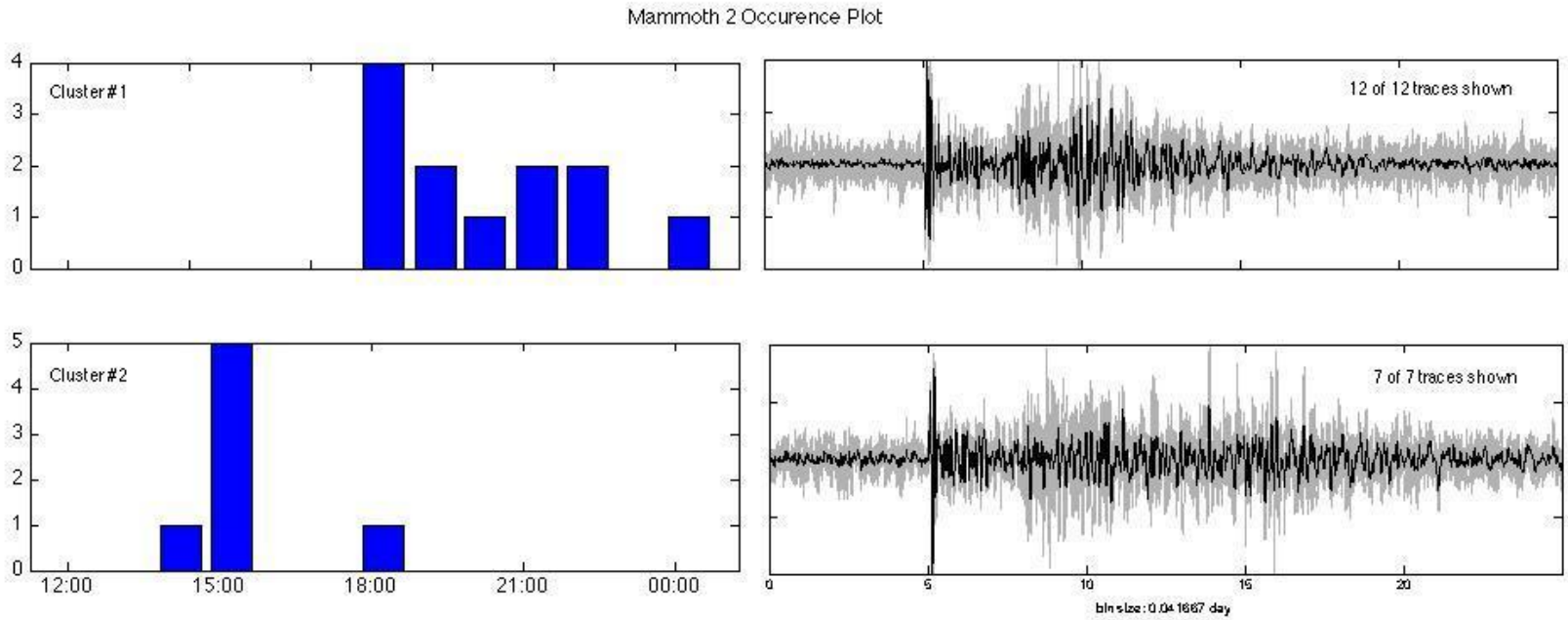

Fig. 26. Occurrence plot of Mammoth IM 2. There is approximately one hour of overlap where one event in cluster 2 occurs during the time when cluster 1 is occurring.

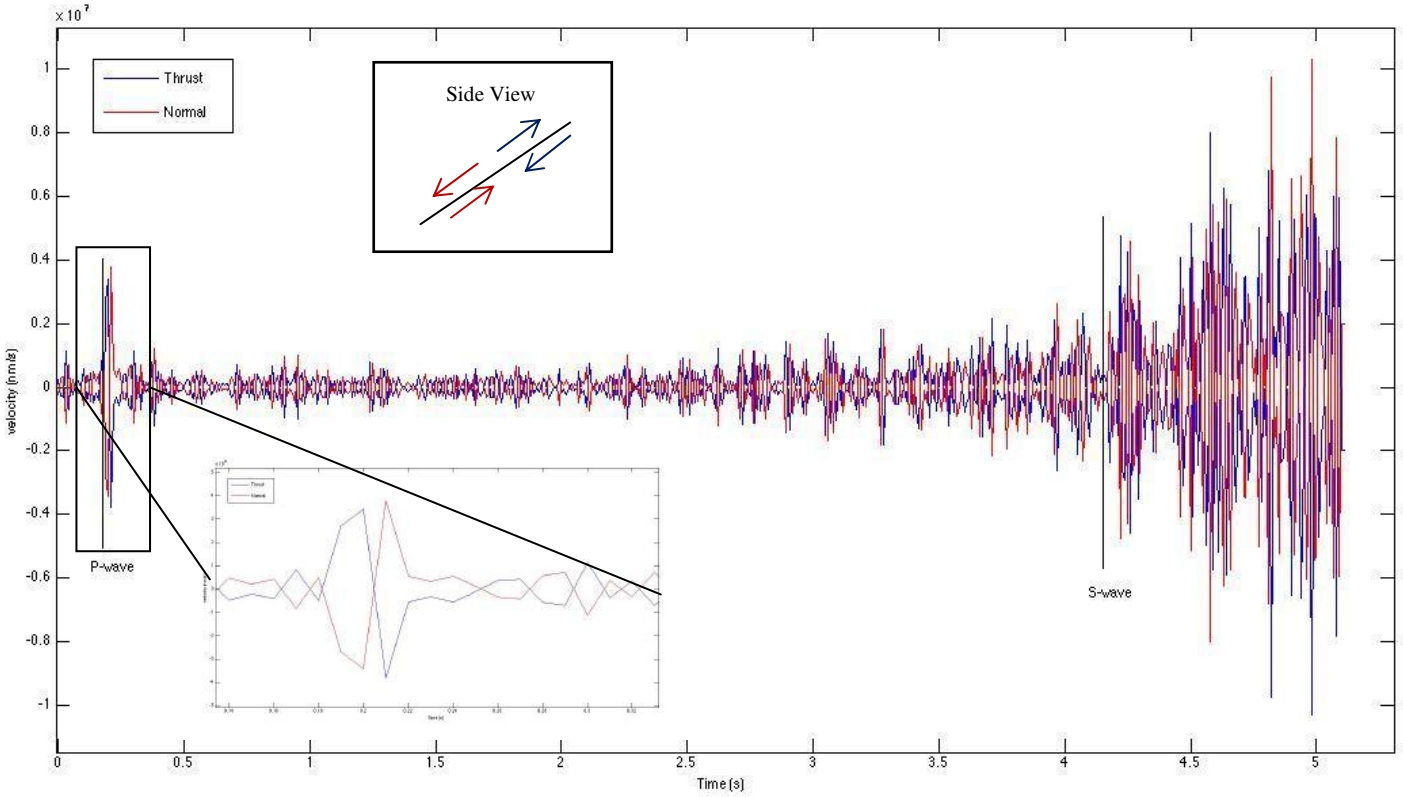

Fig. 27. Two synthetic earthquake waveforms, one with pure thrust motion and one with pure normal motion. Strike of fault is directly north, dip is 45 degrees. Recorded by station 5 km from epicenter, 30 degree azimuth. Correlation coefficient of -1.

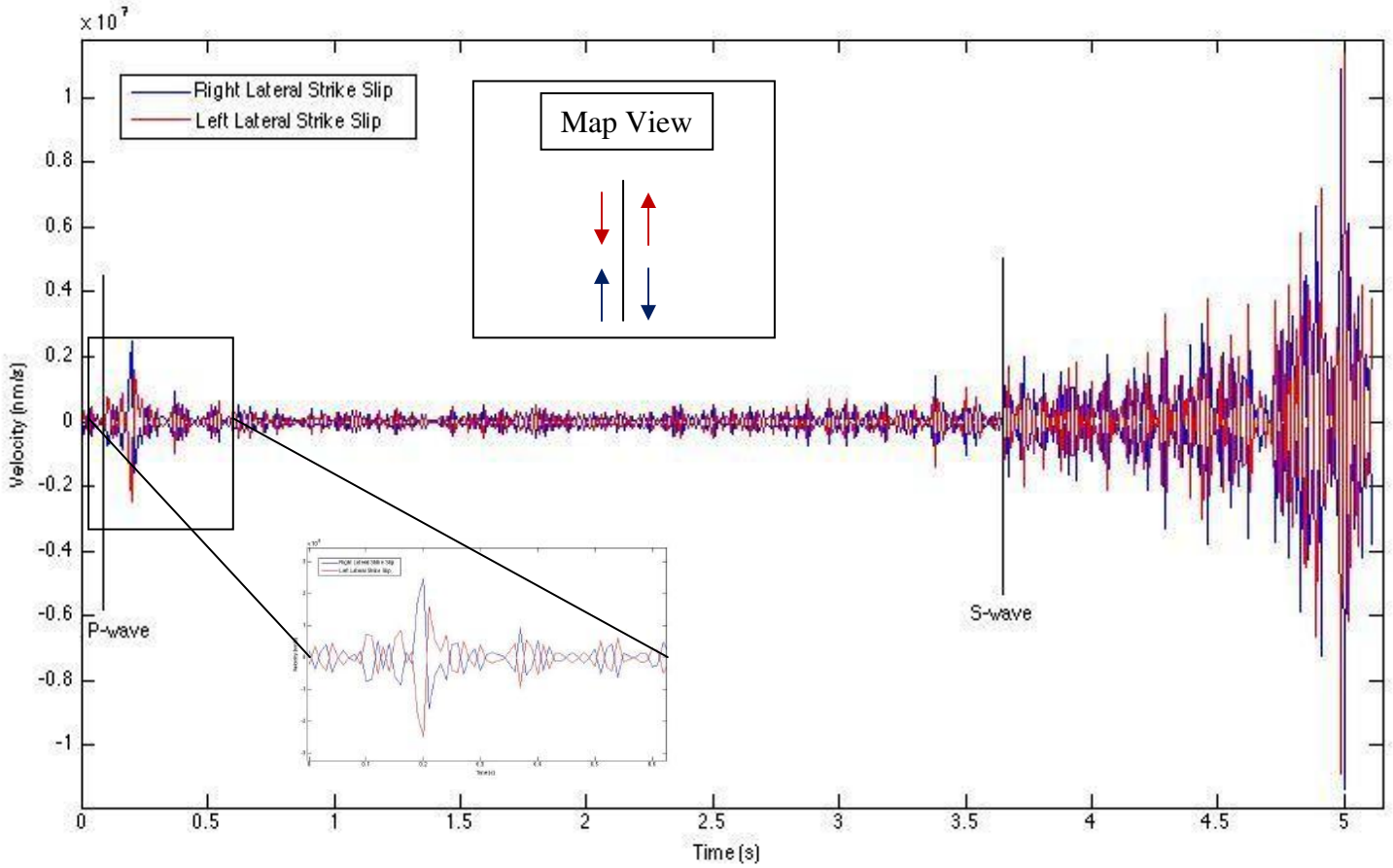

Fig. 28. Two synthetic earthquake waveforms: one caused by right lateral strike slip motion and one caused by left lateral strike slip motion. Recorded by station 5 km from epicenter in 30 degree direction. Correlation coefficient of -1.

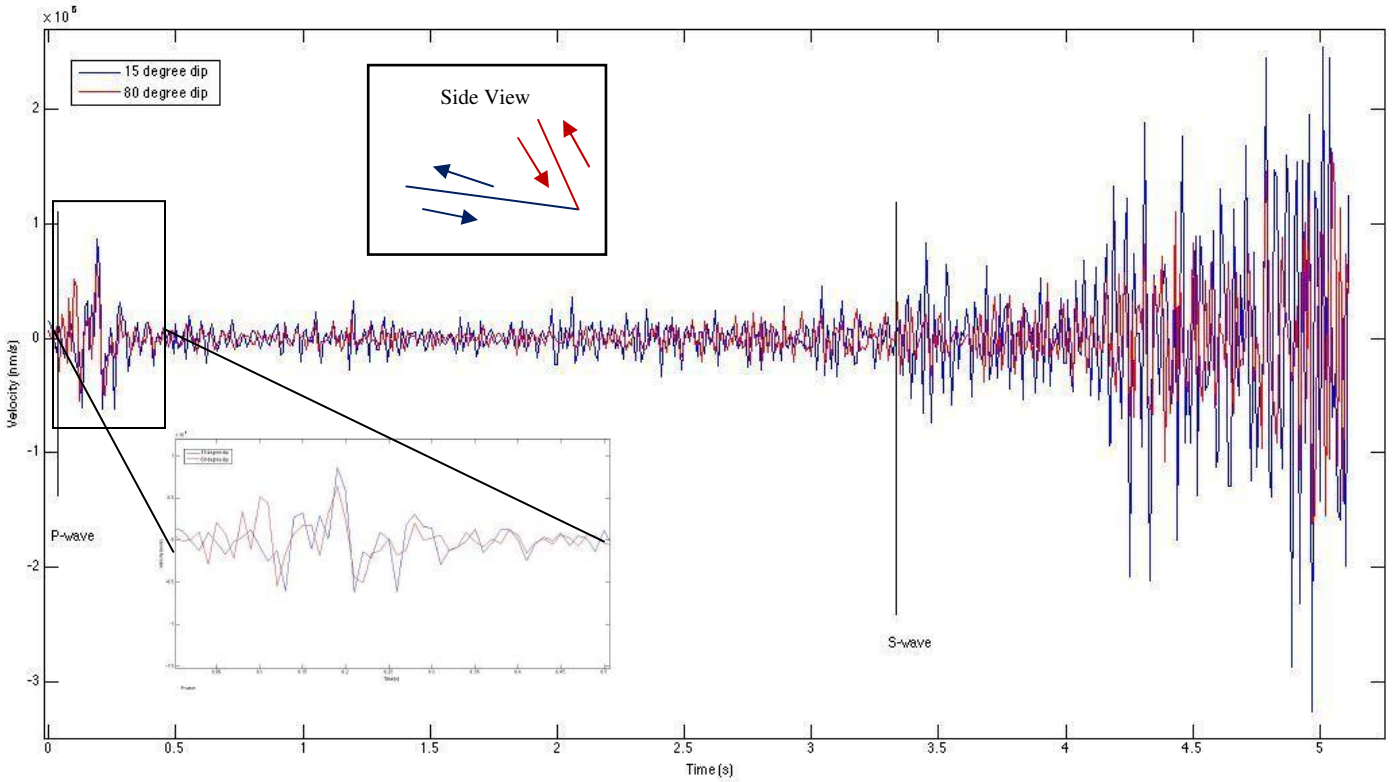

Fig. 29. Two synthetic earthquake waveforms with different dips. Strikes are directly north. Recorded by seismometer 5 km from the epicenter in the 30 degree direction. Correlation coefficient of 0.24 across the entire waveform. While the P-wave correlation is higher, at 0.69, it is still not sufficient to be considered a multiplet.

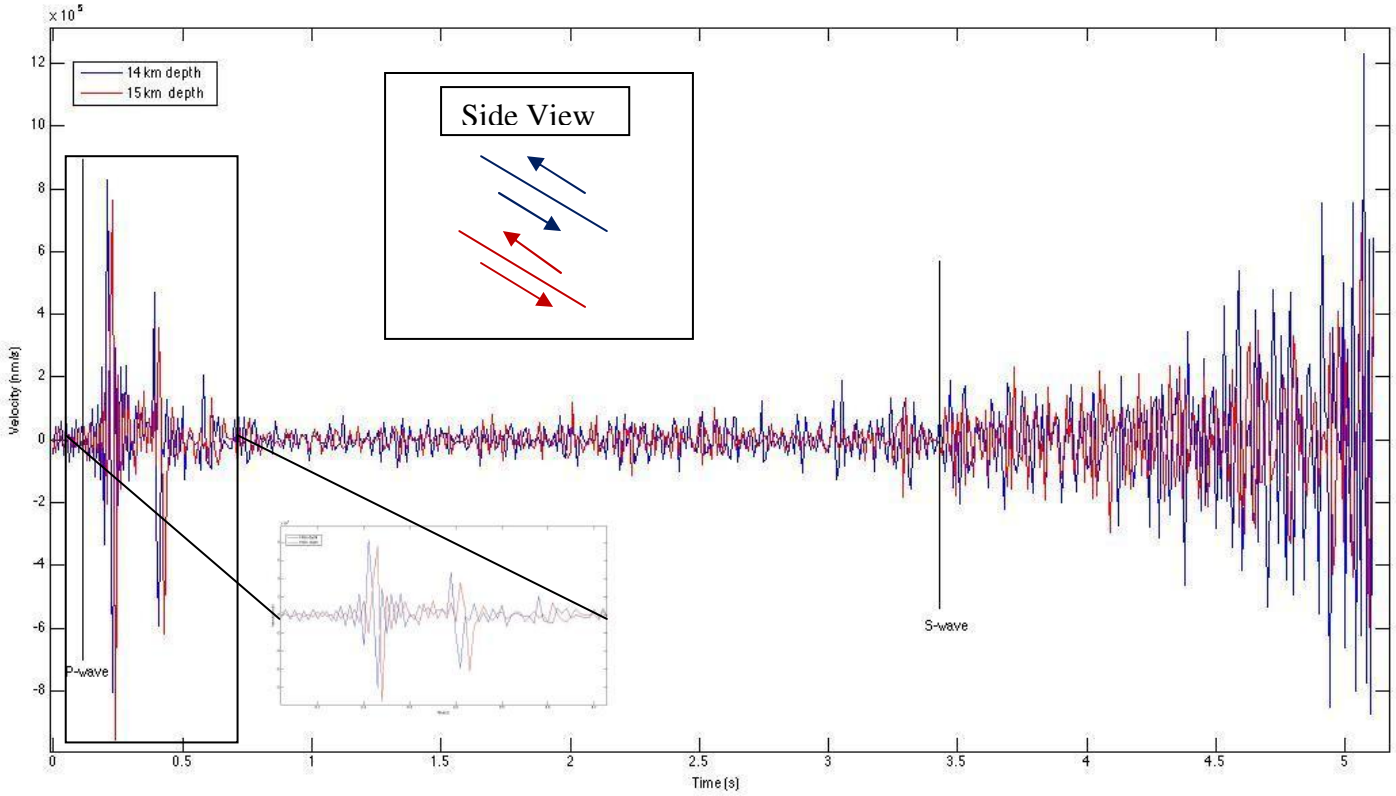

Fig. 30. Two synthetic thrust earthquakes, one at 14 km and one at 15 km depth. Strike is directly north and dip is 45 degrees. Recorded by seismometer 5 km from epicenter at a 30 degree azimuth. Correlation coefficient of -0.34.